1967-12

A Study of the Vertical Motions and of the Diabatic Heating Effects in the Lower Stratosphere During Early April 1963.

Rogers, Will

Monterey, California. Naval Postgraduate School

UNITED STATES
NAVAL POSTGRADUATE SCHOOL

THESIS

A Study of the Vertical Motions and of the Diabatic Heating Effects in the Lower Stratosphere During Early April 1963

by

Will Rogers, Jr.

[redacted]

A STUDY OF THE VERTICAL MOTIONS AND OF THE DIABATIC HEATING EFFECTS IN THE LOWER STRATOSPHERE DURING EARLY APRIL 1963

by

Will Rogers, Jr.
Lieutenant, United States Navy
B.S., University of Washington, 1959

Submitted in partial fulfillment of the
requirements for the degree of

MASTER OF SCIENCE IN METEOROLOGY

from the

NAVAL POSTGRADUATE SCHOOL
December 1967

Signature of Author Will Rogers Jr.

Approved by F. L. Martin
Thesis Advisor

G. J. Haltiner
Chairman, Department of Meteorology
and Oceanography

R. F. Rinehart
Academic Dean

ABSTRACT

Based on a vertical motion model derived by Martin (1964), and applied by Jarrell (1967), a method is developed for producing diabatic heating function fields at 50 mb from independently computed fields of diabatic and adiabatic vertical motion. Vertical motions over and above the adiabatically computed part are found to be of major significance in the diabatic heating function calculations. The resulting heating function fields are shown to be compatible with existing synoptic trends at 50 mb and above, for the data period 1-5 April 1963. A proposed circulation linkage involving ozone-heating areas is advanced, which fits all of the mean zonal computations of diabatic heating and of vertical motion into a consistent pattern.

TABLE OF CONTENTS

LIST OF TABLES

LIST OF ILLUSTRATIONS

LIST OF SYMBOLS AND ABBREVIATIONS

Cp	Specific heat of air at constant pressure (1.00464 j/gm/^{o}K)
$\dot{Q}$	Differential of heat with respect to time (δH/dt)
Wg	Geostrophic vector wind
K	R/Cp = 0.28571
α	Specific density (1/ρ)
Θ	Potential temperature
σ_H	Holl stability parameter
$\tilde{U}$	12-hour time mean value of U
$\overline{U}$	Five-day time mean of U
[U]	Zonal mean of U
$\underline{X}$	Geopotential thickness parameter
∇	Finite difference del operator
gpm	Geopotential meters
j	Joules
gm	Grams
m	Meters*
cm	Centimeters
ω_A	Adiabatic vertical motion in (x,y,p,t) coordinates
ω_D	Diabatic vertical motion in (x,y,p,t) coordinates
Δ_t	12-hour "time difference"
NMC	National Meteorological Center
FNWF	Fleet Numerical Weather Facility
CDC	Control Data Corporation
T	Temperature
p	Pressure
Z	Contour height at a pressure surface

η	Absolute vorticity
f	Corolis parameter
ω	Vertical motion in (x,y,p,t) coordinates
ρ	Density
t	Time
χ	Velocity potential function
ψ	Stream function
∇	Horizontal gradient, del operator
∇^2	Laplacian operator
g	Acceleration due to gravity (9.80665 m/sec^2)
R	Gas constant for dry air (0.28704 $j/gm/^oK$)
d	Mesh length (381 km at 60^oN)
m	Map factor* $(1 + \sin 60^o)/(1 + \sin \phi)$
ϕ	Latitude
i	Grid column number
j	Grid row number
Φ	Geopotential ($\Phi = gz$)
$\mathbb{J}$	Finite difference Jacobian operator without grid distance divisor
∇^2	Finite difference Laplacian operator without grid distance divisor

* Where map factor and meters appear together, meters will be denoted mtr.

ACKNOWLEDGEMENT

The many difficulties and disappointments encountered in the preparation of this paper have only been exceeded by the encouragement and, in many cases, invaluable assistance from the staff and faculty of the Naval Postgraduate School. All of their names cannot be listed here, but it must be said that without their support this paper would have been impossible. However, special mention must be made of the essential computer programming assistance from Lieutenant Commander D. Chin, USN. The willing cooperation of FNWF personnel and, in particular, Mr. L. C. Clarke, is gratefully acknowledged. Also, the writer is indebted to Assistant Professor J. D. Mahlman for his many helpful and discriminating suggestions regarding the final manuscript. But more than anyone else, Professor F. L. Martin has made this paper possible. He has provided the unpublished manuscript on which this study is based, his knowledge and perception constitute whatever substance may be found in the interpretation of the results, and his understanding and patience with this writer have proven to be little short of phenomenal.

1. Introduction

Atmospheric heat budget analysis has become increasingly prominent in the environmental sciences literature of the past decade. The availability of lower stratospheric data has permitted the objective re-examination of previous heating effect theories which were, unavoidably, restricted to global and hemispheric generalizations - beyond the local effects. As the quantity and reliability of such data increases, concepts will gradually lend practical perspective to synoptic scale variations in the development of numerical-prognosis models involving diabatic effects.

Some of the notable investigations on adiabatic heating in the stratosphere during recent years are those of Budyko (2), Davis (4), and Ohring (11). Examples of more specialized investigations leading to synoptic scale applications are those of Jarrell (7), Martin (8), Paulin (13), and Pressman (14). The present study further focuses the attention on the effects of lower stratospheric heating and vertical motion phenomena by investigating the 50 mb diabatic heating function for a time near the spring reversal during April 1963.

Background for the present study began in 1964 when Martin developed a method for obtaining 12-hour mean velocity potential fields. This method was applied to 300, 200, and 100 mb levels for the period 1-5 April 1963 in order to study a time near the spring reversal.

The data utilized by Martin became available from NMC in late 1963, and did not extend above 100 mb. The significance of Martin's diagnostic technique for the present study lies in its application

toward defining vertical motion fields in terms of geopotential, which are generally compatible with the quasi-geostrophic modeling equations [see Arakawa (1)].

Working with Martin, Jarrell produced 50 mb vertical motion fields using a method which will be discussed below. These omega fields are based directly on Martin's χ-fields for 1-5 April 1963, and constitute one of the basic inputs to this study.

Recently, 30 and 50 mb fields of both temperature and geopotential (official analyses of the Air Weather Service) have become available for the same time and in the same format as the data used by Martin; that is, the octagonal 1977-point NMC grid. This new data will be utilized, in addition to Jarrell's omega fields, to compute diabatic heating function fields, which can then be used to determine zonally averaged heat transfer mechanisms.

2. Vertical motions at 50 mb

Martin's process involved the numerical solution of the balance equation

$$\nabla\cdot(f\nabla\psi) + 2\left[\frac{\partial^2\psi}{\partial x^2}\frac{\partial^2\psi}{\partial y^2} - \left(\frac{\partial^2\psi}{\partial x\partial y}\right)^2\right] = \nabla^2\Phi \qquad (1)$$

to produce nondivergent, rotational stream function fields in terms of geopotential, $\Phi = gz$. By iterative solution of

$$\tilde{\eta}\nabla^2\tilde{\chi}^{(n)} = -\left[\nabla^2\frac{\partial\tilde{\psi}}{\partial t} + \tilde{J}(\tilde{\psi},\tilde{\eta})\right] - \tilde{\nabla}\tilde{\eta}\cdot\tilde{\nabla}\tilde{\chi}^{(n-1)} \qquad (2)$$

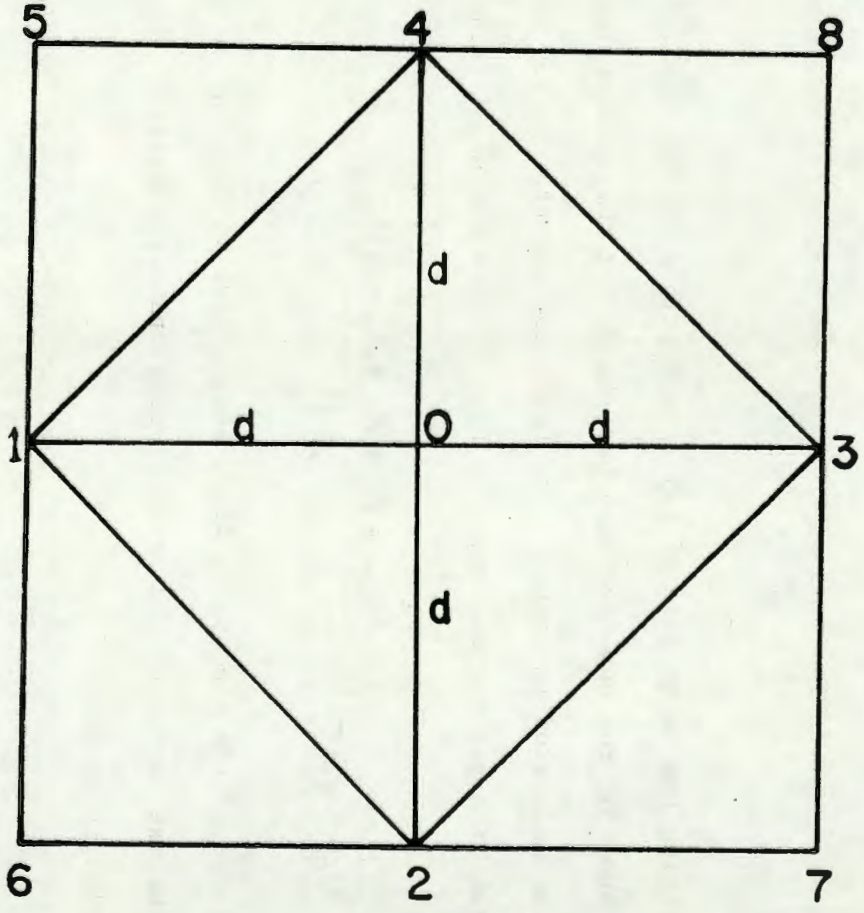

FIG. 1. The finite differencing grid.

Martin solved for 12-hour mean potential fields for 0600GMT and 1800GMT at 100, 200, and 300 mb levels for 1-5 April 1963. The term in the brackets of (2) was the forcing function, and was known at each map time from the solution of (1).

In an effort to determine vertical motions at 50 mb, Jarrell obtained smoothed divergence fields from

$$\nabla \cdot \tilde{\tilde{\mathbb{V}}} = \nabla^2 \tilde{\tilde{\chi}} \tag{3}$$

computing the right side of (3) from Martin's stored $\tilde{\tilde{\chi}}$-fields. In (2) and (3), the superior wavy bar stands for the time centered value of the indicated parameter. The Laplacian operator in (3) was applied to the nine point grid shown in Fig. 1, with the usual format

$$\nabla_9^2 \tilde{\tilde{\chi}} = m^2 \left(\frac{\chi_5 + \chi_6 + \chi_7 + \chi_8 - 4\chi_0}{2d^2} \right) \tag{4}$$

in terms of the nine point differencing mesh of Fig. 1. In (4), m is the map factor of the polar stereographic projection. Next, the continuity equation

$$\nabla_p \cdot \mathbb{V} = - \frac{\partial \omega}{\partial p} \tag{5}$$

was integrated to compute vertical velocity fields at 300, 200, 100, and 50 mb. In order to do this, it was necessary to fit $\partial\omega/\partial p$ by a Lagrangian interpolating quartic polynomial. It was further considered appropriate to include the assumption $\partial\omega/\partial p = 0$ at $p = 0$. The resultant ω-fields were then expressible in terms of linear

combinations of $\nabla^2\chi$ at 100, 200, and 300 mb, and maximum values at 50 mb as high as 10 cm/sec resulted. Concerning the validity of the assumption $\partial\omega/\partial p = 0$, there is considerable evidence, particularly by Pantske (12), that both horizontal wind components during the stratospheric reversal are decreasing and in process of reversing sign on a hemispheric scale. Since the reversal normally occurs in mid-April, the assumption $\partial\omega/\partial p = 0$ seems appropriate to this general time, as noted by Jarrell.

Therefore, Jarrell's work has produced thermodynamically unrestricted ω-fields at 50 mb which are suitable for comparison to independently computed ω_A-fields. This comparison will then lead to a solution for diabatic, or ω_D-fields.

3. Diabatic ω-equation

The thermodynamic equation may be written in the form

$$\dot{Q} = c_p \frac{dT}{dt} - \alpha \frac{dp}{dt} \tag{6}$$

Upon expansion of the time derivative and use of the geostrophic approximation for advection, one then obtains

$$\frac{\dot{Q}}{c_p} = \frac{\partial T}{\partial t} + \mathbf{V}_g \cdot \nabla T + \omega\left(\frac{\partial T}{\partial p} - \frac{RT}{c_p p}\right) \tag{7}$$

By employing the hydrostatic consistency condition, $T = -R^{-1}(\partial\Phi/\partial \ln p)$ for temperature in terms of geopotential, and using a potential temperature equivalent for the term in parentheses, eq. 7 becomes

$$-\frac{R}{c_p}\dot{Q} = \frac{\partial^2 \Phi}{\partial t \partial \ln p} + V_g \cdot \nabla \frac{\partial \Phi}{\partial \ln p} + \frac{1}{p}\left(-\frac{RTp}{\theta}\frac{\partial \theta}{\partial p}\right)\omega \qquad (8)$$

This form has been chosen in order to utilize a static-stability parameter introduced by Holl (6) which he defines in the form

$$\sigma_H = -\frac{RTp}{\theta}\frac{\partial \theta}{\partial p} \qquad (9)$$

The use of σ_H is felt to be appropriate because it has been found by Fleet Numerical Weather Facility (FNWF), Monterey, California, to provide vertical consistency between standard analysis levels, while permitting horizontal consistency with randomly introduced wind data. This static-stability parameter may also be written

$$\sigma_H = -RP\frac{\partial T}{\partial p} + \frac{R^2 T}{c_p} = \left[\frac{\partial^2 \Phi}{\partial \ln p^2} - K\frac{\partial \Phi}{\partial \ln p}\right] \qquad K = \frac{R}{c_p} \qquad (10)$$

Since there is a second derivative in (10), σ_H must be treated as a constant over a depth of three successive pressure levels in finite differencing about p = 50 mb. With the finite differencing pressure interval specified as $\ln p_3/p_2 = \ln 30/50$, the third pressure level is taken as p = 83.3333 mb, with p_2 = 50 mb, and p_3 = 30 mb. Since mean temperature, and the thickness equivalent (to be denoted $\bar{X}$) in (15), below, will be shown to be proportional to one another; the choice of the 83.3 mb level is required to "match" 30 mb for an equal logarithmic interval across 50 mb. Geopotentials at 83.3 mb will be obtained by an interpolation process to be discussed later in this section.

For the purpose of expressing σ_H in terms of geopotential, $\Phi = \Phi(p)$ is selected in the form of a quadratic polynomial in terms of ln p, as follows

$$\Phi = \Phi_{50} + a \ln \frac{P}{50} + b \left(\ln \frac{P}{50} \right)^2 \tag{11}$$

By substituting p = 30 and p = 83.3 and adding and subtracting

$$a = - \frac{(\nabla \Phi)_{50}}{2 \ln 5/3} \qquad b = \frac{(\nabla^2 \Phi)_{50}}{2 (\ln 5/3)^2} \tag{12}$$

where

$$\nabla \Phi = \Phi_{30} - \Phi_{83.3} \qquad \nabla^2 \Phi = \Phi_{30} - 2\Phi_{50} + \Phi_{83.3} \tag{13}$$

In (13), $\nabla \Phi$ and $\nabla^2 \Phi$ are the first and second order finite difference operators, in the vertical.

<u>The thickness tendency equation</u>. Because of the greater "noise" in the stratospheric temperature fields available to us, as compared to fields of geopotential, it is advantageous to use geopotential thickness (mean temperature) fields at 50 mb. This is a slightly different stability treatment than that of Craig et al (3) in the study of vertical motions associated with "explosive stratospheric warming". However, the foregoing development obviously calls for the geopotential thickness field approach.

Eq. 8 may now be written

$$\frac{\partial^2 \Phi}{\partial t \partial \ln p} + \mathbf{V}_g \cdot \nabla \frac{\partial \Phi}{\partial \ln p} + \frac{\sigma_H \omega}{P} = - \frac{R}{C_p} \dot{Q} \tag{14}$$

Multiplying each term by $p\,\delta(\ln p)$ and integrating from $p_1 = 83.3$ to $p_3 = 30$ yields

$$\int_{P_1}^{P_3} p\frac{\partial^2 \Phi}{\partial t \partial \ln p}\,\delta \ln p + \int_{P_1}^{P_3} |\nabla_g \cdot p \nabla \frac{\partial \Phi}{\partial \ln p}\,\delta \ln p + \int_{P_1}^{P_3} \sigma_H \omega \delta \ln p = \int_{P_1}^{P_3} -\frac{RP}{C_p}\dot{Q}\,\delta \ln p \qquad (15)$$

Eq. 11 suggests a definition of "thickness" parameter as follows

$$\underline{X} \equiv \int_{P_1}^{P_3} \left(\frac{\partial \Phi}{\partial \ln p}\right) p\,\delta \ln p \qquad (16)$$

so that

$$\underline{X} = \int_{P_3}^{P_1} RTP\,\delta \ln p = R\bar{T}\int_{P_3}^{P_1} P\,\delta \ln p \qquad (17)$$

The last form of the integral (17) has the value of $R\bar{T}(p_1 - p_3) = 53.333\ R\bar{T}$. Thus $\underline{X} = 53.3333\ R\bar{T}$ and is a measure of the mean temperature, and conversely of the geopotential thickness. This confirms the statement made just above eq. 11. From eq. 11, $\partial \Phi / \partial \ln p$ may be written

$$\frac{\partial \Phi}{\partial \ln p} = a\frac{\partial}{\partial \ln p}(\ln p - \ln 50) + b\frac{\partial}{\partial \ln p}\left[\left(\frac{\ln p}{50}\right)^2\right]$$

$$= a + 2b\left(\ln \frac{p}{50}\right) \qquad (18)$$

Then by (16), with p_1, p_2 and p_3 as previously specified, and with a and b as given by (12), $\underline{X}$ is written

$$\bar{\chi} = \left[\frac{\nabla^2 \bar{\Phi}_{50}}{(\ln 5/3)^2} + \frac{\nabla \bar{\Phi}_{50}}{2 \ln 5/3}\right] 53.3 + \frac{\nabla^2 \bar{\Phi}_{50}}{(\ln 5/3)^2}\left(-30 \ln 5/3 - 83.3 \ln 5/3\right) \qquad (19)$$

$$= 34.7297\,\bar{\Phi}_{30} + 34.9478\,\bar{\Phi}_{50} - 69.6775\,\bar{\Phi}_{83.3}$$

in units of gpm(mb), or j(gm)$^{-1}$mb. For purposes of deriving a value for omega at 50 mb it is useful to consider $\bar{\chi}$ as "thickness" throughout this study.

Now eq. 15 may be integrated to produce the diagnostic equation from which adiabatic-omega, ω_A, will result. Considering $\sigma_H(p)$ constant with respect to p in the layer p_1 to p_3 (but not constant with respect to x and y), the result is

$$\frac{\partial \bar{\chi}}{\partial t} + \widetilde{\mathbf{V}_{q_{50}} \cdot \nabla \bar{\chi}} + \tilde{\sigma}_H \tilde{\omega}_{50} \ln \frac{30}{83.3} = -\int_{P_1}^{P_3} \frac{R}{C_p} \dot{Q}\, dp \qquad (20)$$

with $\bar{\chi}$ defined by (16). In (20), a superior wavy bar denotes a 12-hour mean value. In finite difference form, (20) becomes

$$\frac{\Delta \bar{\chi}}{\Delta t} + \frac{m^2}{4fd^2} \tilde{J}\left(\bar{\Phi}_{50}, \bar{\chi}\right) - 1.02164\, \tilde{\sigma}_H \tilde{\omega} = R\left(\frac{\tilde{\dot{Q}}}{C_p}\right) 53.3 \qquad (21)$$

The solution for $\tilde{J}$ and $\tilde{\sigma}_H$ is discussed below.

Note that each term on the left hand side of (21) has units of gpm(mb) (12-hrs)$^{-1}$ so long as $\tilde{\omega}$ is in mb(12-hrs)$^{-1}$. On the right hand side, the column mean heating rate $(\tilde{\dot{Q}})$ will be given units of j(12-hrs)$^{-1}$(gm)$^{-1}$; so that $R\tilde{\dot{Q}}/Cp$ still has units of j(gm)$^{-1}$(12-hrs)$^{-1}$. Therefore, the right hand side of (21) becomes (0.28704)(53.3)$(\tilde{\dot{Q}}/Cp)$ j mb(gm)$^{-1}$ (12-hrs)$^{-1}$. But since g = 980.665 cm(sec)$^{-2}$, (from Ref. 18),

it follows that one joule = 101.9716 gpm gm. Thus to obtain consistent units in both sides of (21), the right hand side must be multiplied by 101.9716, and eq. 21 becomes

$$\frac{\Delta \bar{X}}{\Delta t} + \frac{m^2}{4fd^2} \tilde{\tilde{J}}\left(\Phi_{50}, \bar{X}\right) - 1.02164\, \tilde{\tilde{\sigma}}_H \tilde{\tilde{\omega}} = 1.5538 \times 10^3 \tilde{\tilde{\dot{Q}}} \qquad (22)$$

in units of gpm(mb) $(12\text{-hrs})^{-1}$.

The Jacobian term. The finite difference Jacobian of equations 21 and 22 will have the usual form

$$J\left(\Phi, \bar{X}\right) = \left[\left(\Phi_3 - \Phi_1\right)\left(\bar{X}_4 - \bar{X}_2\right) - \left(\Phi_4 - \Phi_2\right)\left(\bar{X}_3 - \bar{X}_1\right)\right] \qquad (23)$$

where the five point grid is formed from a subset of the nine point configuration shown in Fig. 1. The products formed by the J operator have the units $(\text{gpm})^2$ mb. However, the term $m^2/4fd^2$ is equal to

$$\frac{m^2}{4 \sin \phi} \quad \frac{0.473646 \times 10^{-7} \text{ sec}}{(\text{mtr})^2}$$

where m is, as before, the map scale factor[1] of the stereographic projection. Combination of the units of J in (23) with those of $m^2/4fd^2$ yields

$$\frac{\text{mb } (\text{gpm})^2 \text{ sec}}{(\text{mtr})^2} = 9.80665 \frac{(\text{gpm})\,\text{mb}}{\text{sec}}$$

[1]Where meters and map factor appear together, meters will be denoted by mtr.

since 1 gpm = 9.80665 $(\text{mtr})^2/\text{sec}$. The last statement merely redefines 1 gpm in terms of MKS units. By transforming sec^{-1} to a 12-hour time interval, the Jacobian term has the full form

$$0.50165 \times 10^{-2} \left(\frac{m^2}{\sin\phi}\right)_{ij} \mathcal{J}_{ij}\left(Z_{50}, \Sigma\right) \tag{24}$$

in units of gpm(mb) $(\text{12-hrs})^{-1}$.

Finally, because consecutive 12-hourly data is used, an average Jacobian operator ($\tilde{\tilde{\mathcal{J}}}$) is defined at each grid point.

$$\tilde{\tilde{\mathcal{J}}}_{ij} = \frac{\mathcal{J}_{ij}\left(t - \frac{\Delta t}{2}\right) + \mathcal{J}_{ij}\left(t + \frac{\Delta t}{2}\right)}{2} \tag{25}$$

where Δt = 12-hours.

The static-stability parameter. Eq. 22 contains a time averaged stability parameter ($\tilde{\tilde{\sigma}}_H$) which may be expressed for each map time as

$$\sigma_H = \frac{\nabla^2 \Phi}{(\ln 3/5)^2} - K \frac{\nabla \Phi}{2(\ln 3/5)} \tag{26}$$

consistent with equations 10 and 12; with K = R/Cp. Eq. 26 can then be reduced to the form

$$\tilde{\tilde{\sigma}}_H = 4.1120 \tilde{\tilde{\Phi}}_{30} - 7.6647 \tilde{\tilde{\Phi}}_{50} + 3.5527 \tilde{\tilde{\Phi}}_{83.3} \tag{27}$$

which is the time averaged vertical stability parameter for the layer 83.3 mb to 30 mb. The units of $\tilde{\tilde{\sigma}}_H$ are gpm.

Interpolation of Φ to the 83.3 mb level. Before the previously developed expressions for σ_H and $\bar{X}$ can be computed, $\Phi_{83.3}$ must be known. The synoptic levels of 200, 100, and 50 mb being available; a parabolic fitting considered compatible with (11) is utilized. The resulting expression is a Taylor expansion of Φ (ln p) about p = 100 mb.

$$\Phi_{83.3}(p) = \Phi_{100} + \left(\ln\frac{83.3}{100}\right)\frac{\partial\Phi}{\partial \ln p}\bigg|_{P_{100}} + \frac{1}{2}\left(\ln\frac{83.3}{100}\right)^2\frac{\partial^2\Phi}{\partial(\ln p)^2}\bigg|_{P_{100}} \tag{28}$$

Then, (28) can be expressed in finite difference form and reduced to

$$\Phi_{83.3} = 0.2005\,\Phi_{50} + 0.8178\,\Phi_{100} - 0.0480\,\Phi_{200} \tag{29}$$

Adiabatic ω_A-solution. Equations 27, 19, 24, and 22 may now be assembled to produce the working equation for the solution of ω_A:

$$\begin{aligned} &1.0216\left(4.1120\,\tilde{\tilde{\Phi}}_{30} - 7.6647\,\tilde{\tilde{\Phi}}_{50} + 3.5527\,\tilde{\tilde{\Phi}}_{83.3}\right)\tilde{\tilde{\omega}}_{A\,ij} = \\ &\Delta_t\left(34.7247\,\tilde{\tilde{\Phi}}_{30} + 34.9479\,\tilde{\tilde{\Phi}}_{50} - 69.6776\,\tilde{\tilde{\Phi}}_{83.3}\right) + \\ &0.50165\times10^{-2}\left(\frac{m^2_{ij}}{\sin\phi_{ij}}\right)\tilde{\tilde{J}}_{ij}\left(Z_{50}, \bar{X}\right) \end{aligned} \tag{30}$$

or more simply

$$\omega_{A\,ij} = \frac{\Delta_t\,\tilde{\tilde{\bar{X}}} + 0.50165\times10^{-2}\left(\frac{m^2_{ij}}{\sin\phi_{ij}}\right)\tilde{\tilde{J}}_{ij}\left(Z_{50}, \bar{X}\right)}{1.0216\,\tilde{\tilde{\sigma}}_H} \tag{31}$$

in units of mb(12-hrs)$^{-1}$. Note that $\bar{X}$ is used in two terms, that $\Phi_{83.3}$ must be precomputed, and that 12-hourly averages apply

throughout. The operator Δt is the 12-hour "time-differencer", and Z_{50} is the (dimensionless) contour height of the 50 mb surface.

It should be noted that the advecting wind is the geostrophic wind, rather than the quasi-geostrophic one. Also the static-stability (σ_H) has been allowed to have space variability inherent in its definition, rather than held to a constant atmosphere value. Both of these energy constraint violations could assume major proportions in a prognostic procedure, but are minor in a diagnostic one. The use of σ_H and of geostrophic advection were conveniently adaptable to the use of existing FNWF subroutines.

On the octagonal boundary (ω_A) is taken to be zero at each boundary point. This is equivalent to choosing as boundary conditions

$$\frac{\partial \bar{X}}{\partial t} = 0 \qquad \text{and} \qquad \mathcal{J}\left(Z_{50}, \bar{X}\right) = 0$$

at each boundary point. One grid interval within any boundary point, both $\partial X/\partial t$ and $\mathcal{J}(Z_{50}, \bar{X})$ are well defined, and ω_A is computable as at any other interior grid point.

4. Heating function solution

Eq. 20 may be written

$$\frac{\partial \tilde{\tilde{\bar{X}}}}{\partial t} + \tilde{\tilde{V}}_{g_{50}} \cdot \tilde{\tilde{\nabla \bar{X}}} + \tilde{\tilde{\sigma}}_H \left(\tilde{\tilde{\omega}}_A + \tilde{\tilde{\omega}}_D\right) 1.02164 = \frac{160}{3} \frac{R}{c_p} \tilde{\tilde{Q}} \qquad (32)$$

For the adiabatic case, $\tilde{\tilde{Q}}$ is zero, and $\tilde{\tilde{\omega}}_D$ is zero. By using an unrestricted ω which is independently[2] computed, together with the

[2]Note the "time centered" ω is not defined as in (25), but results from (32).

just computed ω_A, a solution for ω_D is

$$\omega - \omega_A = \omega_D$$

As noted in Section 2, the value of ω will be taken as that computed by Jarrell. By writing (32) for ω and ω_A, subtracting, and using σ_H from (27) we may write

$$\tilde{\tilde{\dot{Q}}}(.2857)\frac{1000}{3} = -1.02164(\tilde{\tilde{\omega}} - \tilde{\tilde{\omega}}_A)(4.1120\tilde{\tilde{\Phi}}_{30} - 7.6697\tilde{\tilde{\Phi}}_{150} + 3.5527\tilde{\tilde{\Phi}}_{833}) \quad (33)$$

A field of $\tilde{\tilde{\omega}}_D$ is formed in units of mb $(12\text{-hrs})^{-1}$ to compute the field of $\tilde{\tilde{Q}}$ at 50 mb in $j(gm)^{-1}(12\text{-hrs})^{-1}$.

Recall that the right side of eq. 22 with $\tilde{Q}$ in $j(gm)^{-1}(12\text{-hrs})^{-1}$ was converted to units consistent with those of (33) by the multiplicative factor 1.5538×10^3. Thus temporarily consider (33) as

$$1.5538\,\tilde{\tilde{\dot{Q}}} \times 10^3 = -1.02164\,\tilde{\tilde{\omega}}_D\,\tilde{\tilde{\sigma}}_H \quad (34)$$

and obtain, upon simplification

$$\tilde{\tilde{\dot{Q}}}_j = -0.6575 \times 10^{-3}\,\tilde{\tilde{\sigma}}_H\,\tilde{\tilde{\omega}}_D \quad (35)$$

In (35), $\tilde{\tilde{\sigma}}_H$ is the expression within the last pair of parentheses of (33), and, of course, is time averaged for each point of the grid, similar to the operation of (25). With $\tilde{\tilde{\omega}}_D$ also in mb(12-hrs), the notation $\tilde{\tilde{Q}}_j$ infers units of j/gm/(12-hrs). Finally, it should be noted that eq. 33 requires the assumption that the sum of the local change and advective change in geopotential thickness is the same whether (32) is written for ω or for ω_A. In support of this

assumption, a heat balance study for 1-5 April 1963 applied to the 100 mb level by McClosky (10) indicated that vertical heat divergence was larger than heat transfer by (1.) horizontal advective and (2.) storage processes by one and three orders of magnitude, respectively. If this is also true at 50 mb, then (35) computes only the $\tilde{\tilde{Q}}$ that is expressed by the vertical motion transfer, which appears to be the dominant contribution.

5. Procedures and initial results

The data grid and ω-boundary effects. The FNWF 1604 (modified) CDC computer was used for all data processing, computations, and grid printing discussed herein. Figs. 2, 3, 4, 5, and 6 for 1 April 1963 at 0600GMT are presented as being typical of any of the ten map times processed in this study. Although the computer input data was initially in the form of a 47 X 51 point octagonal grid, the boundary of the computational octagon was restricted by four grid spaces to one of 39 X 43 mesh size due to anticipated boundary value excursions introduced by ω (discussed by Jarrell). As a result, approximately 10° of peripheral grid coverage was lost. However, the loss is not considered too significant for the purposes of this study, due to the sparse data area involved, and to the remaining grid area, which covers the Northern Hemisphere north of (approximately) 18° latitude.

The above mentioned boundary excursions are evident in the $\tilde{\tilde{\omega}}$-field, as seen in Fig. 2 (after Jarrell), and also in the fields of $\tilde{\tilde{\omega}}_D$ and $\tilde{\tilde{Q}}$ (Figs. 4 and 6, respectively) which depend directly upon Jarrell's 50 mb $\tilde{\tilde{\omega}}$-fields. More recent investigation

FIG. 2. Twelve-hour average map of $\bar{\omega}$ vertically centered at 50 mb for 01 April 1963 at 0600GMT (mb/12-hrs).

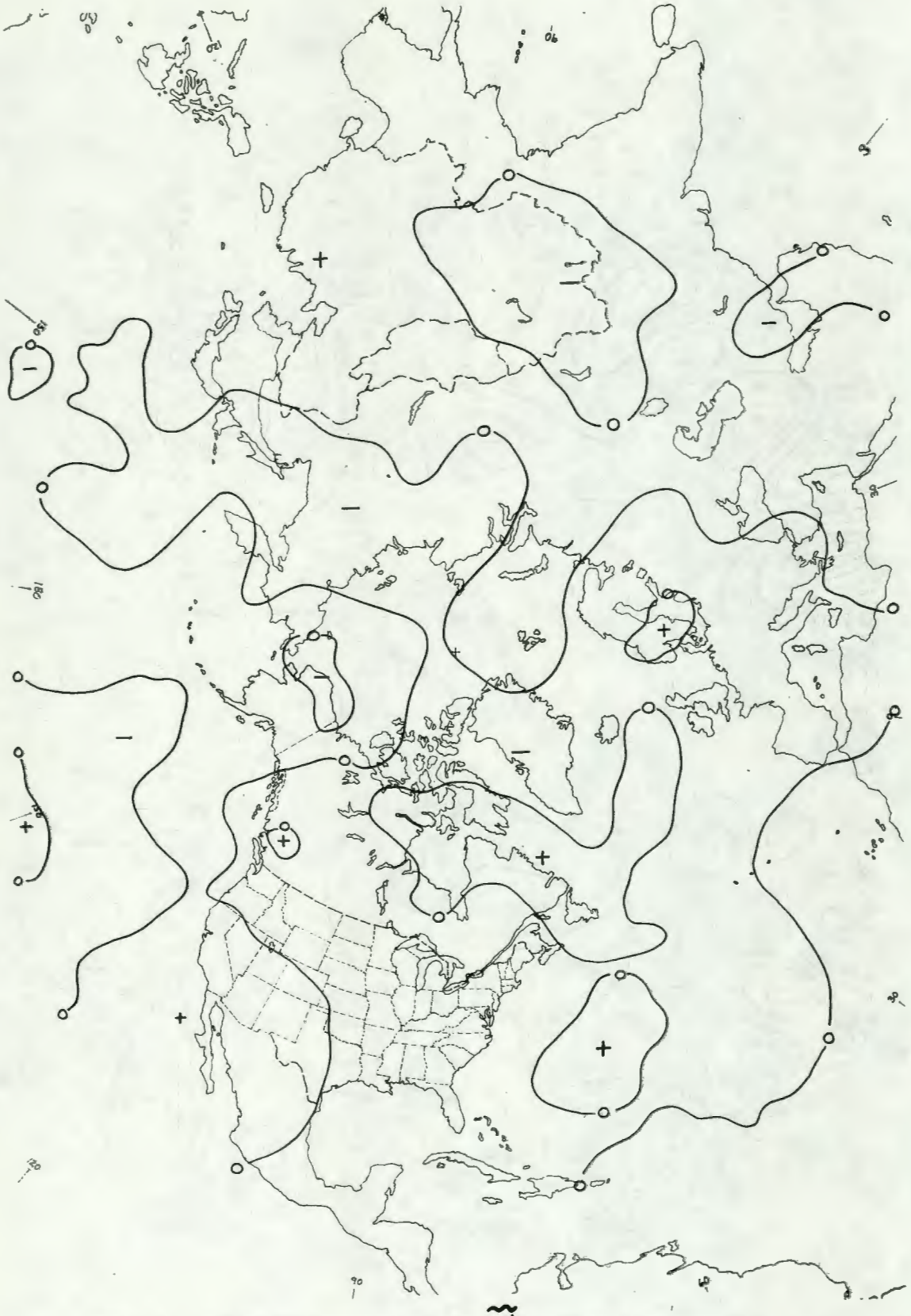

FIG. 3. Twelve-hour average map of $\tilde{\omega}_A$ vertically centered at 50 mb for 01 April 1963 at 0600GMT (mb/12-hrs).

FIG. 4. Twelve-hour average map of $\tilde{\omega}_p$ vertically centered at 50 mb for 01 April 1963 at 0600GMT (mb/12-hrs).

FIG. 5. Twelve-hour average map of $\tilde{\sigma}_H$ vertically centered at 50 mb for 01 April 1963 at 0600GMT (meters).

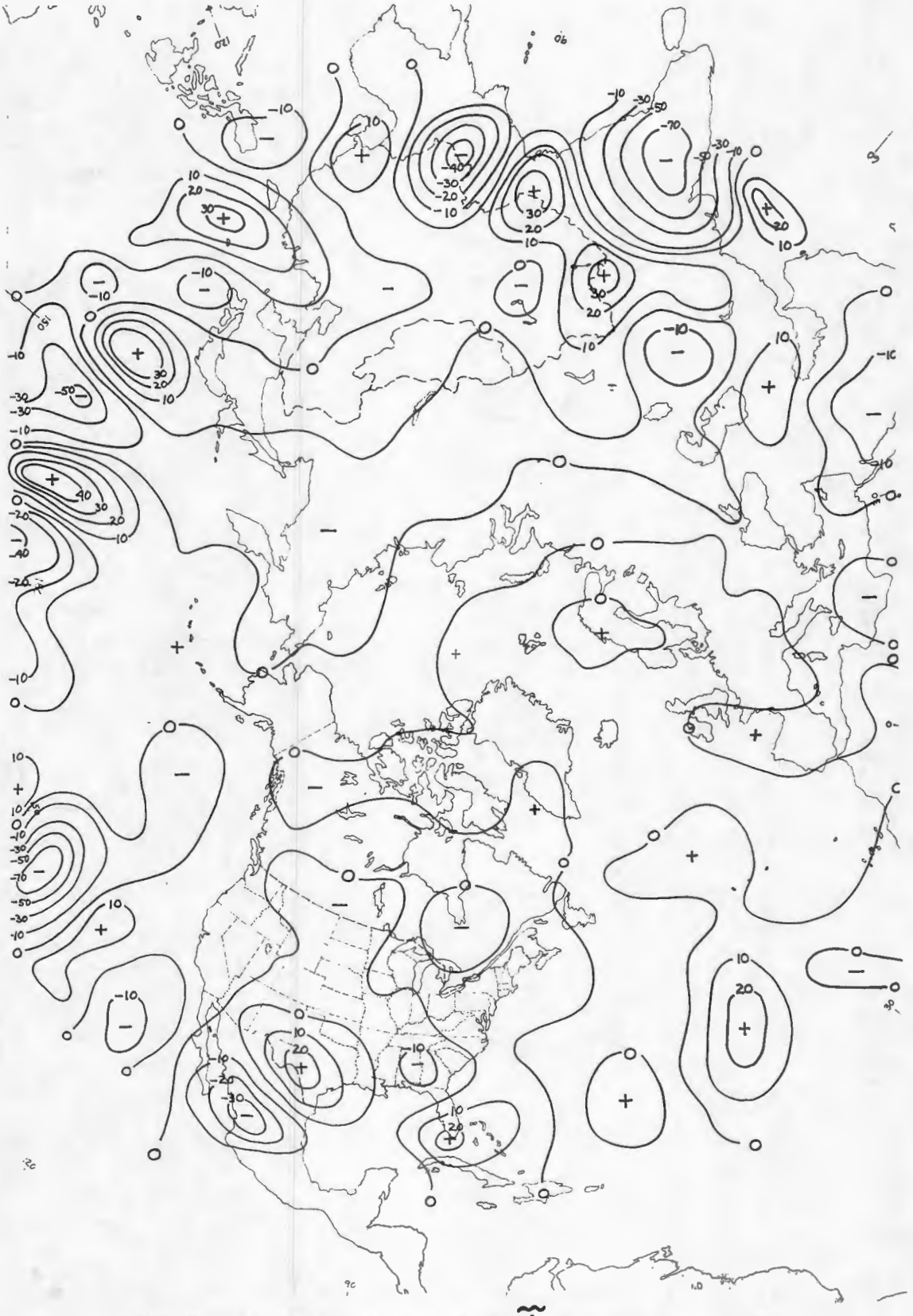

FIG. 6. Twelve-hour average map of $\tilde{\dot{Q}}$ vertically centered at 50 mb for 01 April 1963 at 0600GMT (j/gm/12-hrs)

by Martin[3] (9) promises a marked decrease in the magnitude of this boundary effect on ω, but the revised data fields were not available for this study. The boundary conditions for the ω_A solution of this study simply set $\omega_A = 0$ at all boundary points and this boundary condition led to no apparent excursions in ω_A. However, the $\tilde{\tilde{\omega}}_A$-fields (see Fig. 3), computed by the method of Section 3, have also been "restricted" to the smaller grid of Fig. 5, within which Jarrell's 50 mb ω-values have been considered valid. It is to be recalled that ω_A is computed from eq. 31 within the 47 by 51 octagon.

Away from the boundary zone, the contoured ω-dependent maps for 1 April 1963 at 0600GMT have a regular appearance with a similarity in scale patterns. However, $\tilde{\tilde{\omega}}$ and $\tilde{\tilde{\omega}}_A$ field centers do not coincide. Even with the anomalous ω-values near the boundary, a primary goal of this paper was that of determining the principal meridional heat transfer mechanisms by using, where possible, the zonally averaged quantities $[\omega_D]$, $[\sigma_H]$, $[\dot{Q}]$. In the averaging around latitude bands most of the spurious boundary influences are averaged out.

Presentation of initial results. Fig. 4 shows merely the point-wise subtraction of the fields of $\tilde{\tilde{\omega}}_A$ from $\tilde{\tilde{\omega}}$, of Fig. 2, and the result is the "diabatic" $\tilde{\tilde{\omega}}_D$-field. Fig. 5 shows the field of $\tilde{\tilde{\sigma}}_H$ for the initial time in the sequence. Here $\tilde{\tilde{\sigma}}_H$ is

[3]The proposed approach involves setting the boundary inflow-outflow component of V_χ equal to the divergence of the geostrophic wind at all points centered one row in from the 47 X 51 octagon in a manner similar to that of suppressing "spurious anticyclogenesis" in the ψ-field.

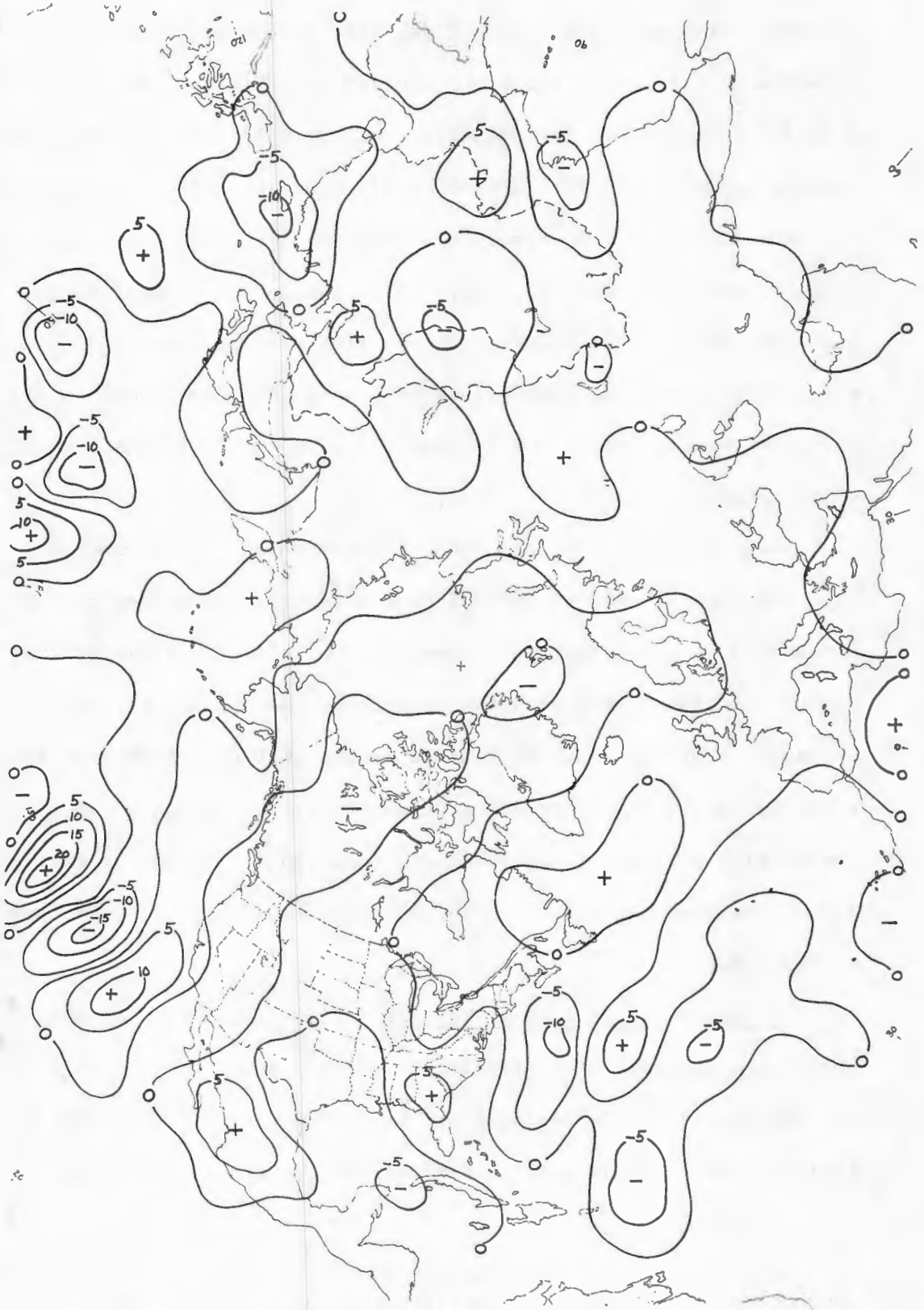

FIG. 7. Five-day mean map of $\bar{\omega}$ vertically centered at 50 mb for 1-5 April 1963 (mb/12-hrs).

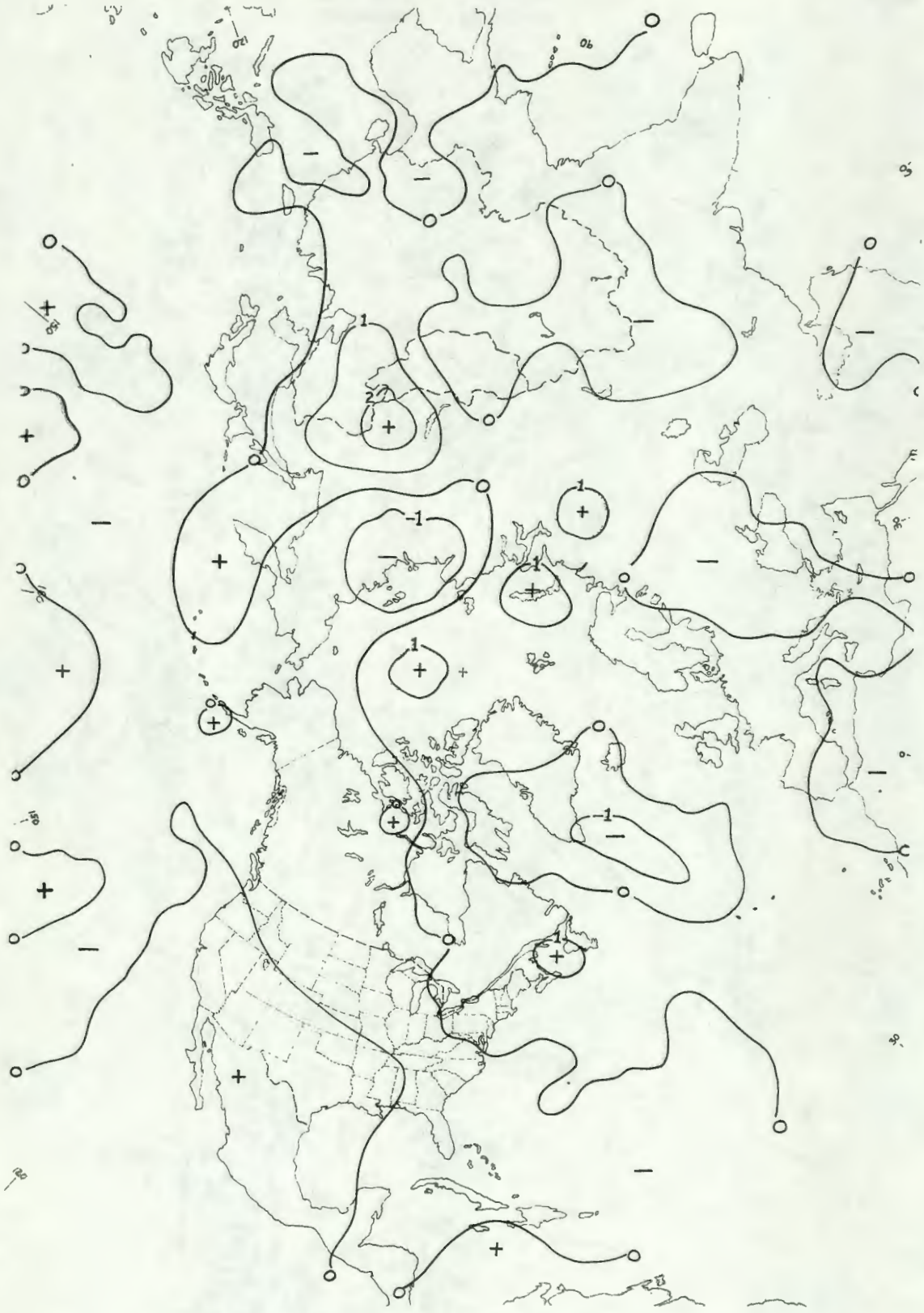

FIG. 8. Five-day mean map of $\overline{\omega}_A$ vertically centered at 50 mb for 1-5 April 1963 (mb/12-hrs).

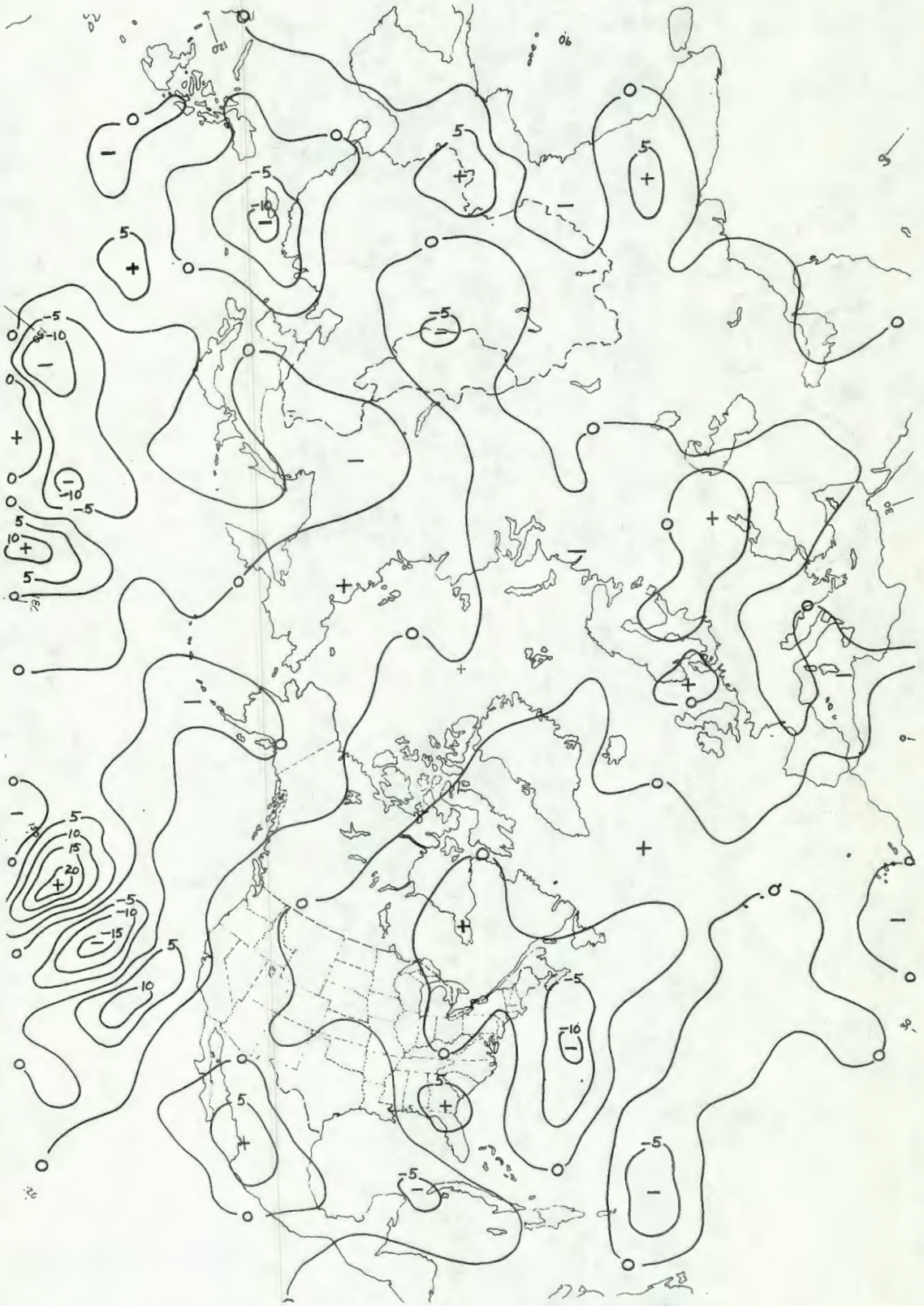

FIG. 9. Five-day mean map of $\overline{\omega}_o$ vertically centered at 50 mb for 1-5 April 1963 (mb/12-hrs).

FIG. 10. Five-day mean map of σ_N vertically centered at 50 mb for 1-5 April 1963 (meters).

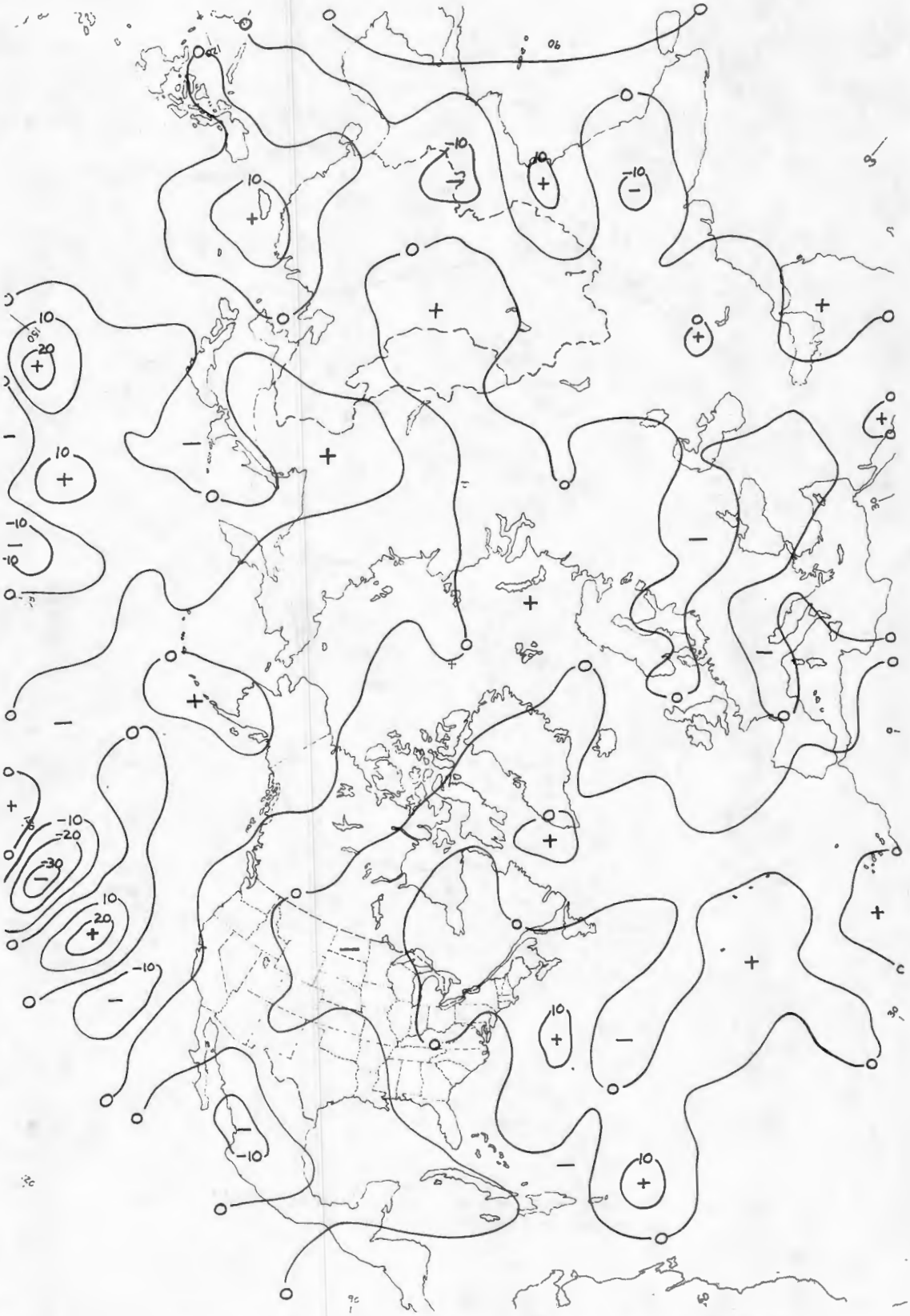

FIG. 11. Five-day mean map of $\overline{Q}$ vertically centered at 50 mb for 1-5 April 1963 (j/gm/12-hrs).

computed at each grid point by eq. 19, but only that portion of the $\tilde{\tilde{\sigma}}_H$ field within the truncated grid has been reproduced, as discussed above. Comparison of Fig. 5 with Fig. 18 [50 mb chart from the analysis series of the Free University of Berlin (15)] shows a remarkable coherency between locations of higher (lower) values of σ_H and the location of warm-ridge (cold-trough) areas; which is a reasonable result.

Fig. 6 shows the first field of computed $\tilde{\tilde{Q}}$ in j/gm/(12-hrs), centered vertically at 50 mb. The computation of $\dot{Q}_{ij}$ at each grid point is based on eq. 35 with the values of $(\tilde{\tilde{\sigma}}_H)_{ij}$ and $(\tilde{\tilde{\omega}}_D)_{ij}$ recalled from the taped records of the applicable data fields.

Similarly, fields of $\tilde{\tilde{\omega}}$, $\tilde{\tilde{\omega}}_A$, $\tilde{\tilde{\omega}}_D$, and $\tilde{\tilde{\sigma}}_H$ were also stored at appropriate grid locations, for each of the other nine map times. Thus a five day mean map was generated for each parameter. These maps are labeled $\bar{\omega}$, $\bar{\omega}_A$, $\bar{\omega}_D$, $\bar{\sigma}_H$ and $\bar{Q}$ in Figs. 7-11 respectively. The superior bar denotes a five day time-mean. In the following sections, the bracket notation enclosing any of the above fields will denote its zonal mean.

6. Zonal means

Computational procedures. Zonal averages by 5° latitude bands were computed for each parameter listed in Table 1. A FNWF subroutine was utilized for obtaining zonally averaged values centered at 20°N, 25°N$\cdots 90^\circ$N. Then all ten fields of each parameter were averaged together to produce the results seen in Table 1. The "average" for the pole point is simply the computed average value for that point weighted with the four surrounding points. A separation of 0600GMT

	20°	25°	30°	35°	40°	45°	50°	55°	60°	65°	70°	75°	80°	85°	90°
$[\bar{\omega}]$	+.24	+.20	+.06	-.04	-.22	-.25	+.01	+.12	+.03	-.09	-.16	-.07	+.14	+.32	+.54
$[\bar{\omega}_A]$	+.05	+.05	+.03	+.01	-.02	-.01	+.08	+.15	+.09	-.07	-.24	-.11	+.34	+.62	+.68
$[\bar{\omega}_D]$	+.19	+.15	+.02	-.04	-.20	-.24	-.07	-.03	-.06	-.02	+.09	+.04	-.20	-.31	-.15
$[\bar{\sigma}_H]$	2881	2554	2175	1987	1699	1333	1190	1246	1240	1200	1347	1553	1624	1504	1227
$[\bar{\dot{Q}}]$	-.35	-.29	-.08	+.03	+.18	+.22	+.06	+.03	+.05	+.01	-.09	-.03	+.22	+.32	+.12

TABLE 1. Zonal means at 50 mb by five degree latitude bands for 1-5 April 1963. All parameters are five day averages: $[\bar{\omega}]$ is the vertical velocity, $[\bar{\omega}_A]$ is the adiabatic vertical velocity, $[\bar{\omega}_D]$ is the diabatic vertical velocity, $[\bar{\sigma}_H]$ is the vertical stability parameter, and $[\bar{\dot{Q}}]$ is the diabatic heating function.

zonal means from those at 1800GMT to permit a possible diurnal investigation was not attempted since the sample was not considered large enough.

Inspection of a preliminary version of Table 1 revealed single-point sign reversals of $[\overline{\omega}]$, $[\overline{\omega_D}]$, and $[\overline{\dot{Q}}]$ at 30°N and 50°N. Whether these sign reversals indicated actual transitory surges, or computational outgrowths of unrepresentative data, is not known. Since these were small perturbations superimposed on larger latitudinal-scale patterns, a one-pass spherical smoother (described below) was applied to the preliminary table.

In order to smooth an arbitrary function of latitude, $U = U(\phi)$, the Laplacian was applied to the one dimensional array $U_i(\phi)$,

$$[\overline{U}_i]_s = [\overline{U}]_i + \tfrac{1}{4} \nabla_s^2 [\overline{U}](a\Delta\phi)^2 \qquad (36)$$

where ∇_s^2 is the spherical finite difference form of the Laplacian. The azimuthal and radial terms of the full spherical Laplacian are not applicable, so that eq. 36 contains only a zonal differencing term of form

$$\frac{1}{a^2 \cos\phi} \frac{\partial}{\partial\phi}\left(\cos\phi \frac{\partial U}{\partial\phi}\right)$$

Thus the values of Table 1 have been adjusted according to

$$[\overline{U}_i]_s = [\overline{U}_i] + \tfrac{1}{4}\left([U_{i+1}] - 2[U_i] + [U_{i-1}]\right) - \tfrac{1}{8}\left([U_{i+1}] - [U_{i-1}]\right)\tan\phi_i \frac{5\pi}{180} \qquad (37)$$

where "i" increases toward the pole, and the smoothing angle between successive i values is $5\pi/(180)$ radians. The "end point" values at $\phi = 20^\circ$, and at $\phi = 90^\circ$ were not subjected to smoothing, although

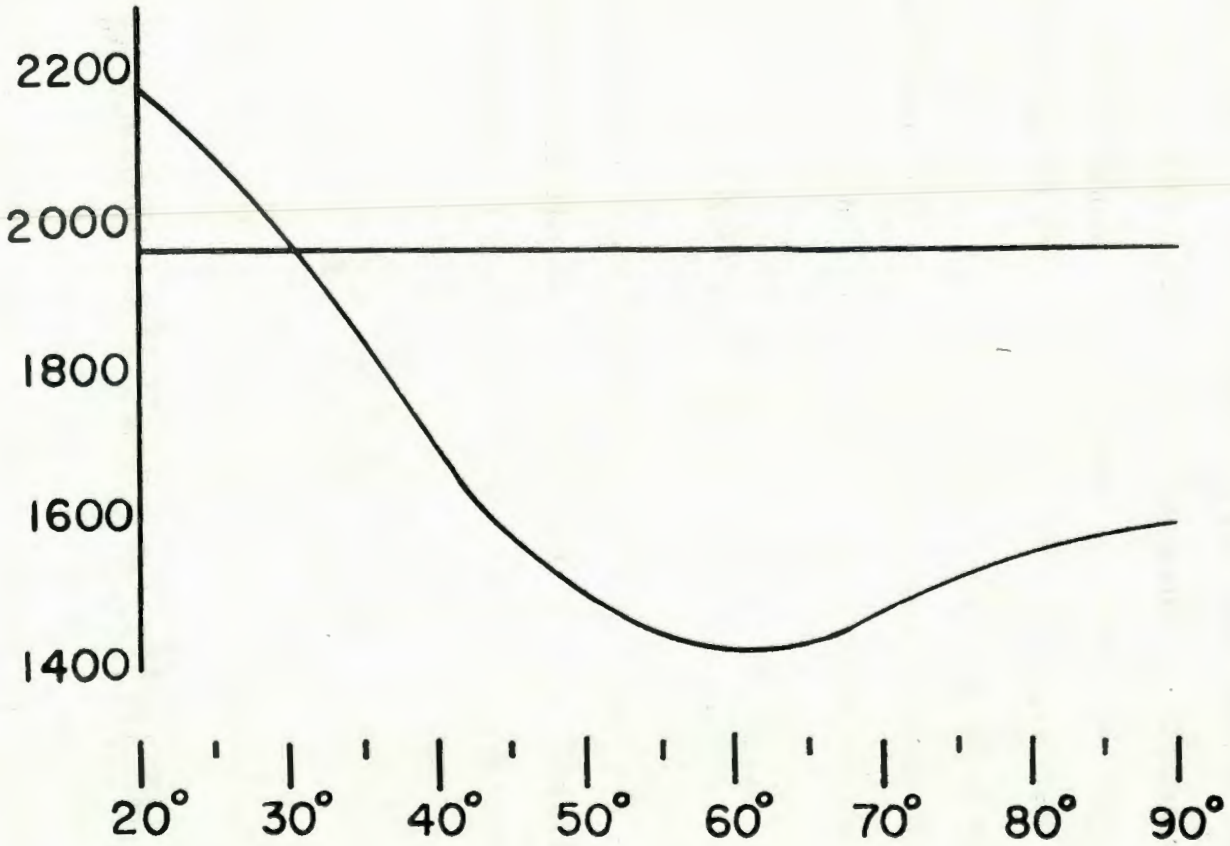

FIG. 12. Graph of five-day mean stability parameter by five degree latitude bands for 1-5 April 1963 (meters). Horizontal line at 1971 meters is the standard value, using eq. 27 and standard geopotential heights from Ref. 18.

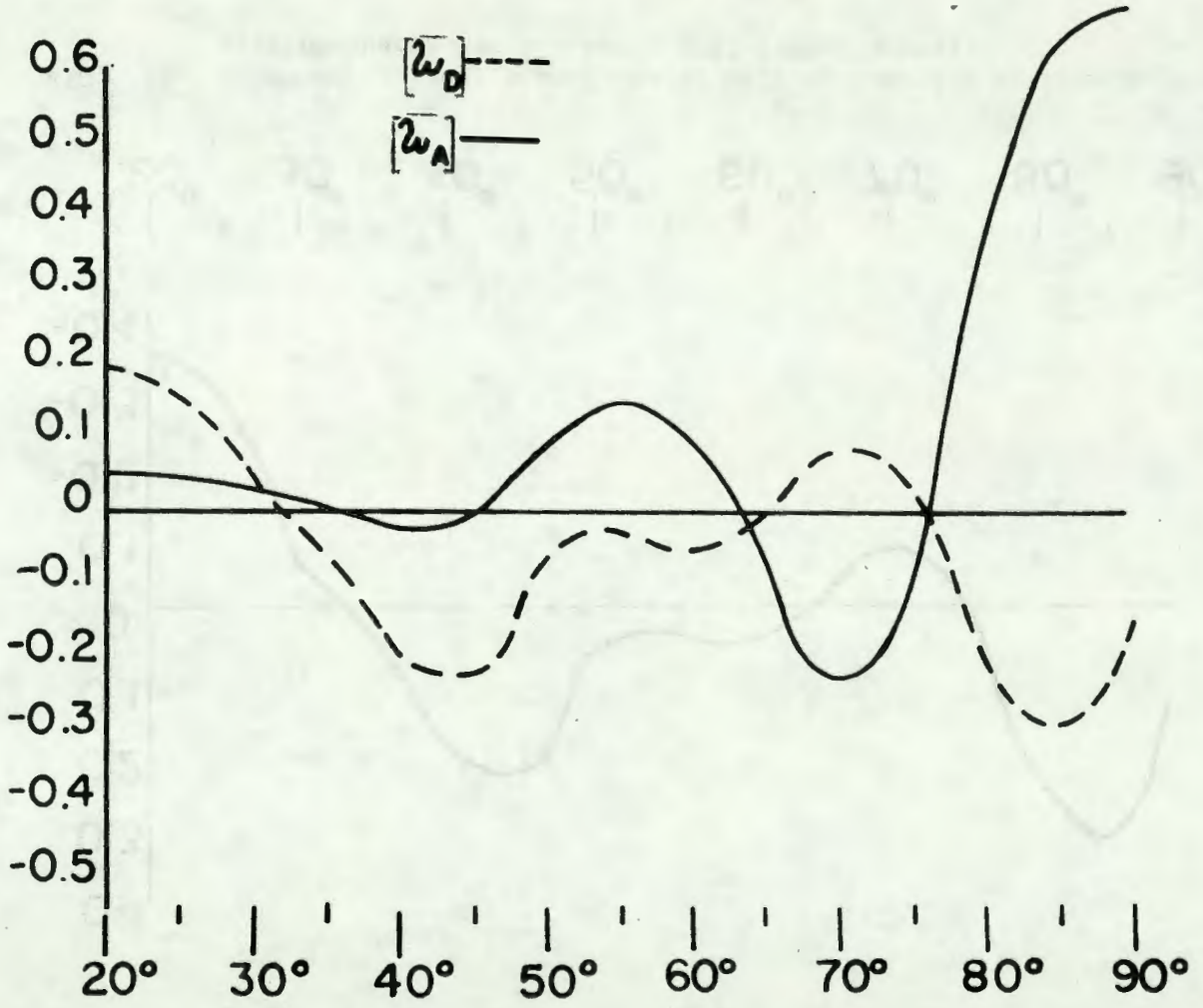

FIG. 13. Graph of five-day mean vertical motion parameters by five degree latitude bands for 1-5 April 1963 (mb/12-hrs).

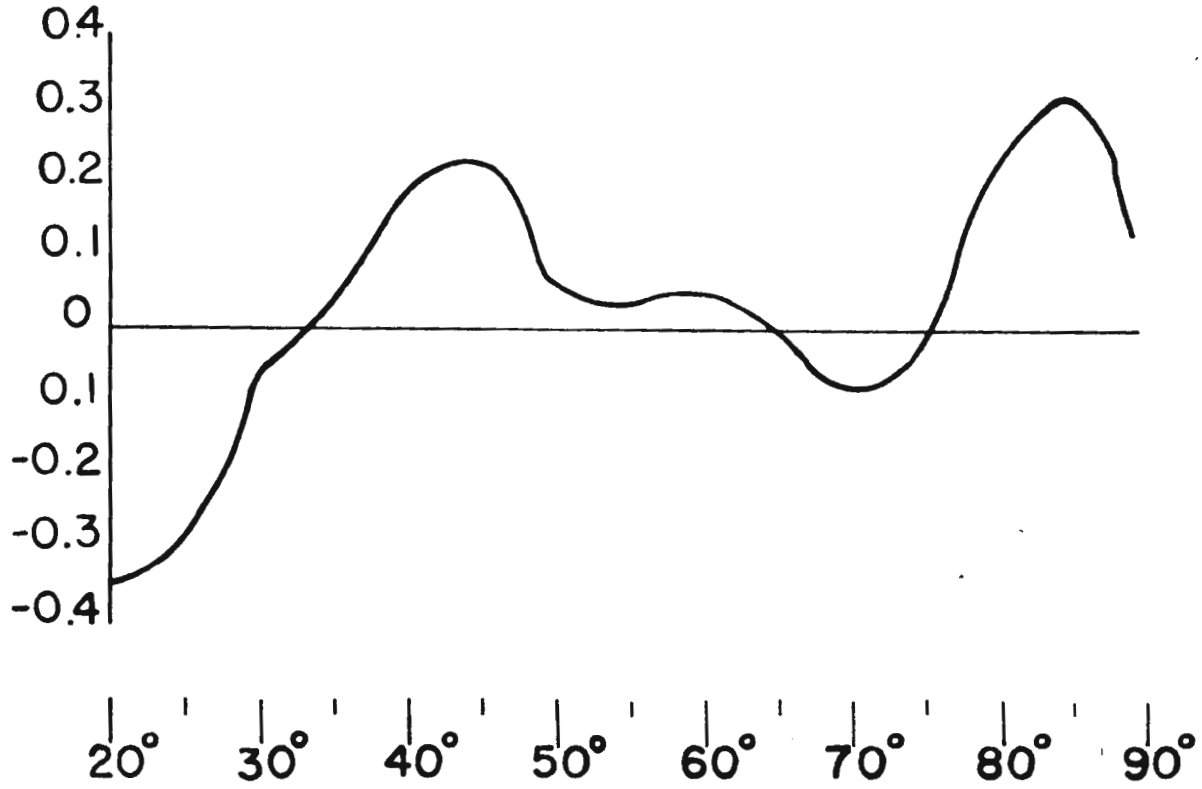

FIG. 14. Graph of five-day mean diabatic heating function by five degree latitude bands for 1-5 April 1963 (j/gm/12-hrs).

as with all other entries in Table 1, they were time averaged.

In order to interpret the most essential aspects of Table 1, $[\overline{\sigma_H}]$, $[\overline{\omega_A}]$ and $[\overline{\omega_D}]$, and $[\overline{\dot{Q}}]$ are graphed on a latitude scale in Figs. 12, 13, and 14, respectively. Note that singular departure points are not present in Table 1, or in the associated graphs; and meridional patterns are evident in all of the tabulated parameters.

7. Zonal mean eddy heat-flux and mean-cellular heat-flux convergences

Since $\dot{Q}$ is expressible by means of eq. 35, it follows that the zonally averaged $[\dot{Q}]$ is expressible as

$$[\dot{Q}] = -K[\sigma_H][\omega_D] - K[\sigma_H^* \omega_D^*] \qquad K = 0.6575 \times 10^{-3} \qquad (38$$

at each latitude, and for each map time. The first term on the right is the contribution of the meridional circulation flux convergence (denoted $\dot{Q}_c$) common to the latitude band. The second term is then ascribed to eddy flux convergence of heat (denoted $\dot{Q}_e$), resulting mainly from synoptic scale systems. Since $[\dot{Q}]$ and $-K[\sigma_H][\omega_D] = [\dot{Q}_c]$ were known for each map time and latitude, the eddy flux term $[\dot{Q}_e] = -K[\sigma_H^* \omega_D^*]$ in (38) was computed as a function of latitude and map time. Then the values of $[\dot{Q}_e]$ and $[\dot{Q}_c]$ were time averaged and smoothed in the same manner as the Table 1 parameters. The resulting five-day zonal mean values are presented in Table 2 under the headings; "cellular" and "eddy flux convergence contributions to $[\overline{\dot{Q}}]$ ". The $[\overline{\dot{Q}}]$ values from Table 1 are reprinted in Table 2 to facilitate comparison with $[\overline{\dot{Q}_c}]$ and $[\overline{\dot{Q}_e}]$.

It would also be possible to perform a time mean analysis of $[\overline{\dot{Q}}]$ in terms of the time mean values of the right side of (38), and

	20°	25°	30°	35°	40°	45°	50°	55°	60°	65°	70°	75°	80°	85°	90°
$[\bar{Q}]$	-.35	-.29	-.08	+.03	+.19	+.22	+.06	+.03	+.05	+.01	-.09	-.03	+.22	+.32	+.12
$[\bar{Q}_c]$	-.27	-.21	-.05	+.04	+.21	+.25	+.06	+.02	+.06	+.02	-.08	-.02	+.22	+.31	+.13
$[\bar{Q}_e]$	-.08	-.08	-.03	-.01	-.02	-.03	-.00	+.01	-.01	-.01	-.01	-.01	-.00	+.01	-.01

TABLE 2. Zonal means at 50 mb by five degree latitude bands for 1-5 April 1963. All parameters are five-day averages: $[\bar{Q}]$ is the diabatic heating function, $[\bar{Q}_c]$ is the cellular flux convergence contribution to $[\bar{Q}]$, and $[\bar{Q}_e]$ is the eddy flux convergence contribution to $[\bar{Q}]$.

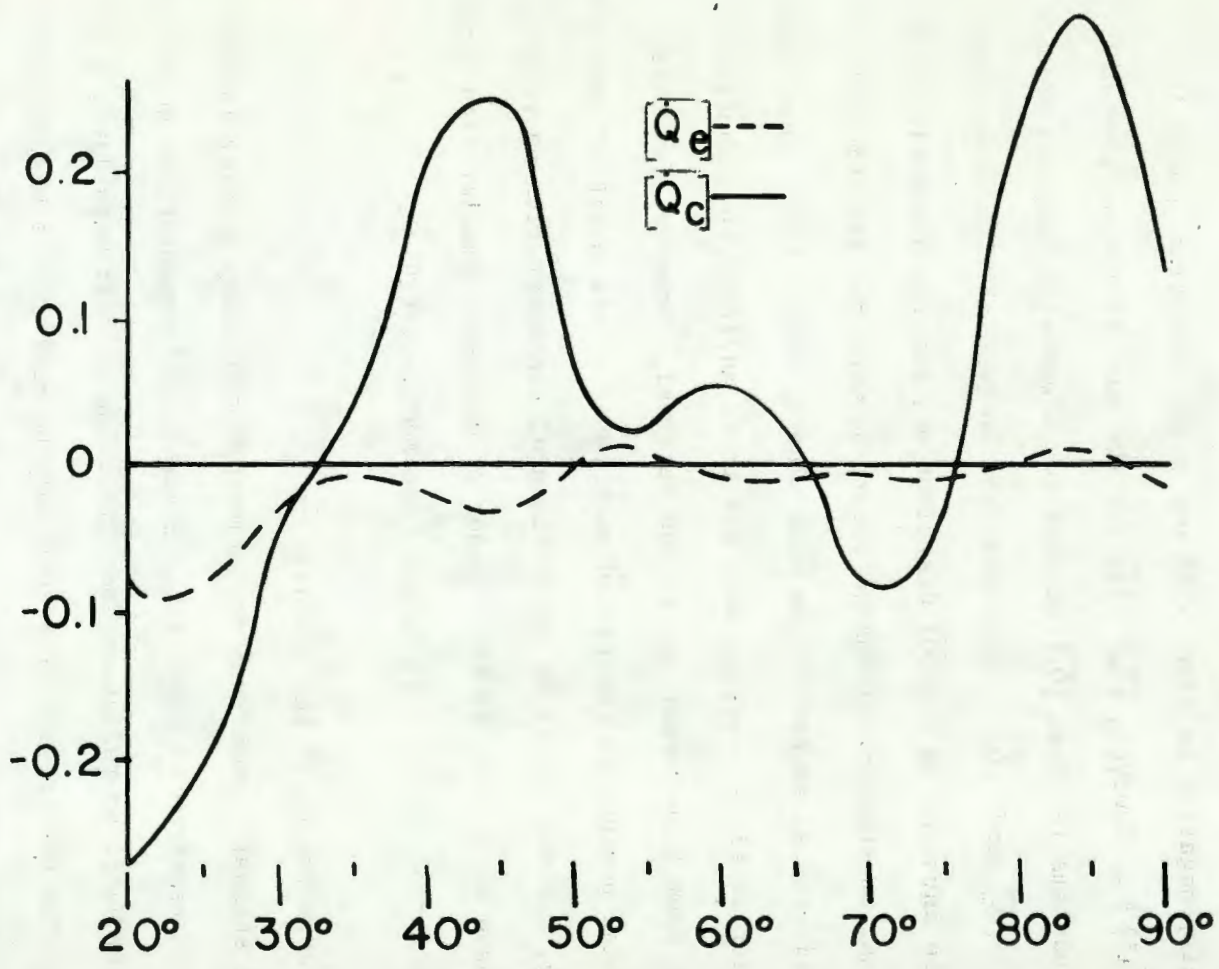

FIG. 15. Graph of five-day mean diabatic heating function parameters: $[\dot{\overline{Q}}_c]$ is the cellular flux convergence contribution to $[\dot{\overline{Q}}]$, and $[\dot{\overline{Q}}_e]$ is the eddy flux convergence contribution to $[\dot{\overline{Q}}]$.

of their transitory flux transports. However, the transitory aspect of these terms has been subordinated to that of determining the two time-averaged distributions of vertical flux convergences, which have been graphed as functions of latitude in Fig. 15.

The results of the $[\overline{Q_e}]$ computation indicate that it is generally negative in sign, with one minor exception [near 50°N (Fig. 15)]. However, $[\overline{Q_e}]$ is, for the most part, an order of magnitude smaller than $[\overline{Q_c}]$ so that for diagnostic purposes we may equate $[\overline{Q_c}]$ and $[\overline{Q}]$. Note that the horizontal flux convergence could be involved in the $[\overline{Q}]$ distribution, but the assumption was made that no substantial change occurs between the diabatic and adiabatic cases; an assumption made also by Paulin (13). Hence the $[\overline{Q}]$ distributions assessed here are those additive contributions arising from transformations in the vertical. However, for this particular period, as contrasted with cases of the onset of explosive warming, maximum values of the horizontal transport flux convergence terms have been found to be an order of magnitude smaller than those resulting from vertical exchanges [see McClosky (10)].

8. Interpretation of the results

A standard comparison for atmospheric heating studies is the excellent research of Davis (4). Since Davis' computations were primarily based on radiation and climatological air mass data, a comparison with the present study can only be made if its results are regarded as deviations from the mean April computations of Davis.

Values presented by Davis for ten degree latitude bands from 20°N to 70°N, are taken as mid-band averages, converted to j/gm/12-hrs,

DAVIS

25°	35°	45°	55°	65°	75°	85°
-.068	-.179	-.280	-.350	-.403		

THIS STUDY

25°	35°	45°	55°	65°	75°	85°
-.254	+.038	+.176	+.041	+.001	-.005	+.269

TABLE 3. Averaged April 1963 heating rates at 50 mb in ten degree latitude bands (j/gm/12-hrs).

and listed in Table 3 from 25°N to 65°N. These values are based on a column centered at 40 mb, but are felt to be sufficiently representative of 50 mb for the purposes of this comparison. The values listed in Table 3 for "this study" are taken from Table 2, using a three point averaging technique of the form

$$[\dot{\bar{Q}}]_{\phi_i} = \frac{\cos\phi_{i-1}[\dot{\bar{Q}}]_{i-1} + 2\cos\phi_i[\dot{\bar{Q}}]_i + \cos\phi_{i+1}[\dot{\bar{Q}}]_{i+1}}{\cos\phi_{i-1} + 2\cos\phi_i + \cos\phi_{i+1}} \qquad (39)$$

where ϕ_i increases poleward in five degree increments.

It is seen that the (30-day average) values taken from Davis call for cooling in all latitude bands, and with magnitudes steadily increasing poleward. In comparison, the (five day average) results of this study show a larger cooling rate in the subtropics, and warming throughout most of the remaining hemisphere. The subtropical cooling rate, however, is representative in sign only, due to the ω boundary value effect at this latitude. The relatively small cooling rate centered near 70°N is quite definite (see Figs. 14 and 15), but is terminated poleward by the strong warming centered near 85°N.

Further investigation reveals that an extrapolation of Davis' infrared cooling and solar heating rates apparently undergo a reversal by mid-April, presumably near the 35 km level [see Figs. 2 and 3, and Table 4; Davis (4)]. However, it would be impossible to infer from such an extrapolation, the latitudes of preferred energy input at levels below 35 km, since the climatological smoothing eliminates any possible consideration of radiation-dynamics in the stratosphere. A hemispheric radiational study to explain the 50 mb warming effects

FIG. 16. Deviations of the April 1963 absolute topography from the 50 mb mean for 1949-53 (geopotential dekameters).

for the period of this study (Figs. 14 and 15) was too prodigious a task to perform with the same degree of detail utilized in the thermodynamic computations employed herein. Moreover, many data gaps exist on a daily basis, which cannot be smoothed over as in a purely climatological approach.

Therefore, the alternative of a judicious synoptic comparison has been attempted, in order to find out how much the data sample of 1-5 April 1963 differs from synoptic stratosphere climatology, and whether these differences are compatible with the 50 mb $[\overline{Q}]$ distribution resulting from this study.

The synoptic charts to be utilized are those from the series published by the Free University of Berlin (15), (16), (17). Fig. 16 illustrates the mean 50 mb height anomalies for the month of April 1963. The developing Arctic anticyclone was more prominent than normal, as was the subtropical belt of high pressure. However, a considerably greater anomaly is obvious in the strong negative height deviations which dominate the Central Asian and North American areas. These negative anomalies are particularly characteristic of actual conditions during the period of this study, as evidenced by Fig. 18 and 19. The southward movement of the subpolar vortices should be noted, as well as the general broadening of the associated trough areas. These trough areas have major southwest and southeast extensions from the corresponding coastal areas of both continents in the vicinity of 45° latitude. This feature is evident on the mean April map of Fig. 17, but is particularly prominent during the data period of 1-5 April. For reasons which will be discussed below, a major significance of these trough areas is their vertical extent <u>above</u> 50 mb.

FIG. 17. Mean absolute topography of the 50 mb surface for April 1963 (geopotential dekameters).

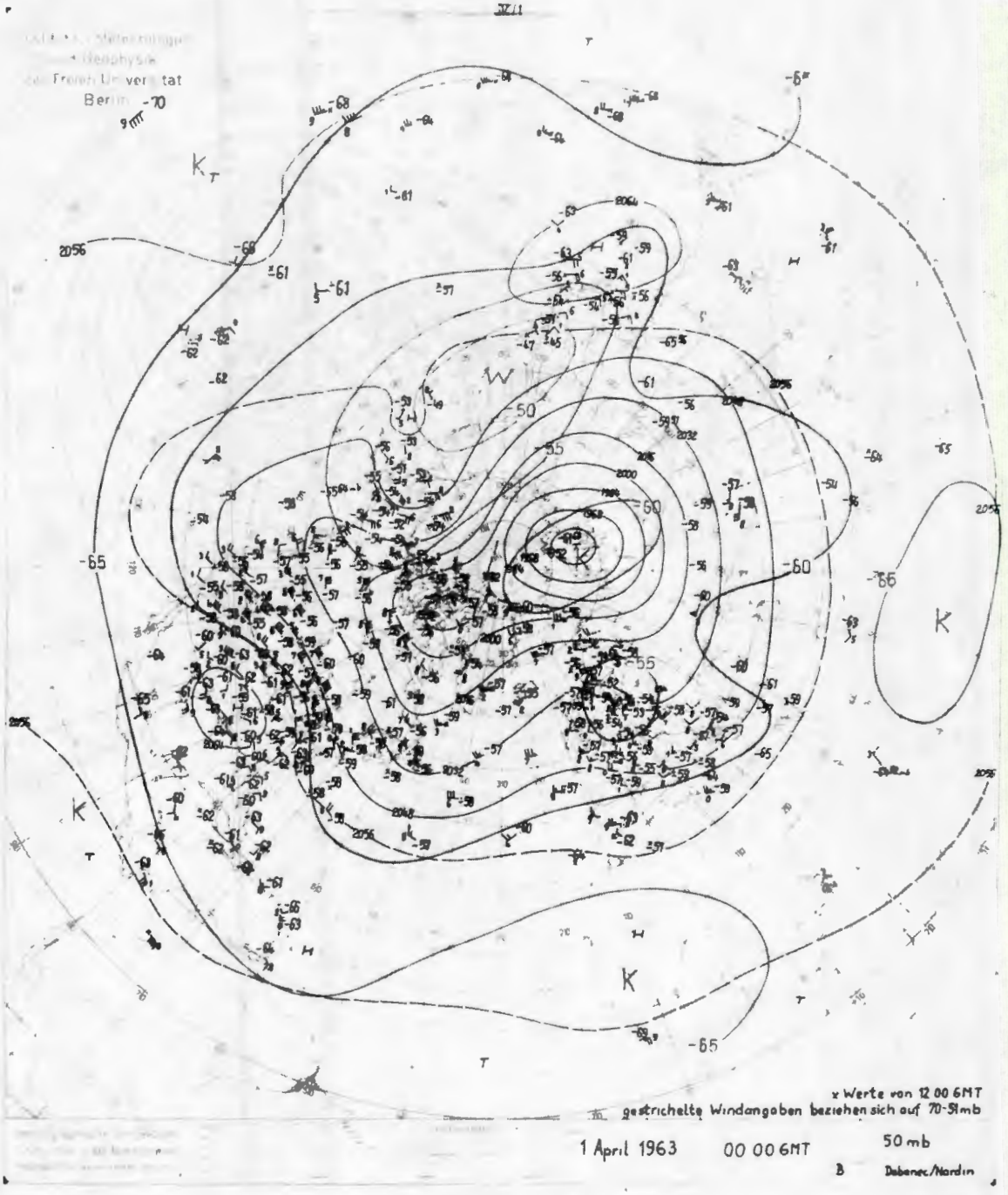

FIG. 18. 50 mb height analysis for 01 April 1963 at 0000GMT (geopotential dekameters).

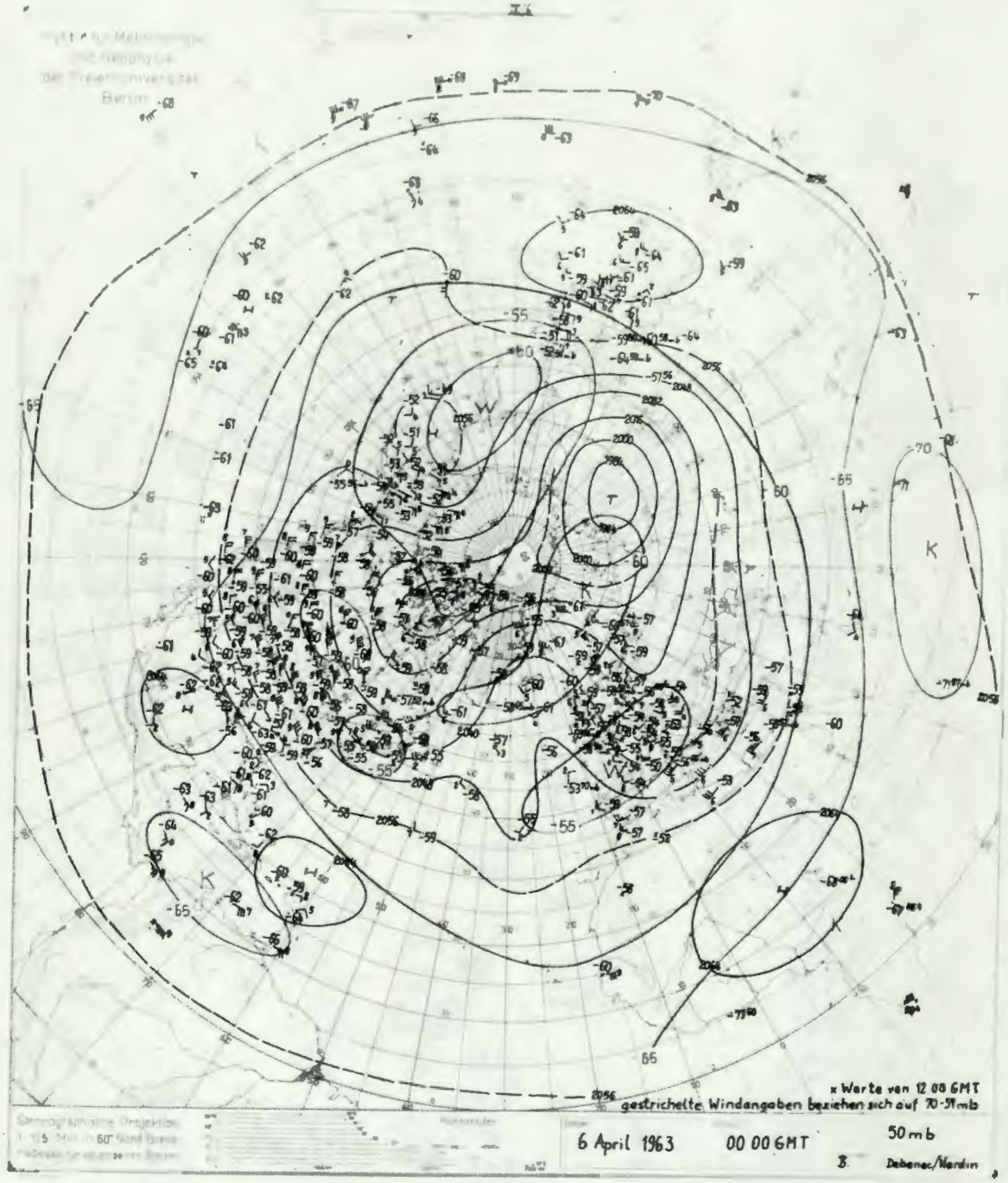

FIG. 19. 50 mb height analysis for 06 April 1963 at 0000GMT (geopotential dekameters).

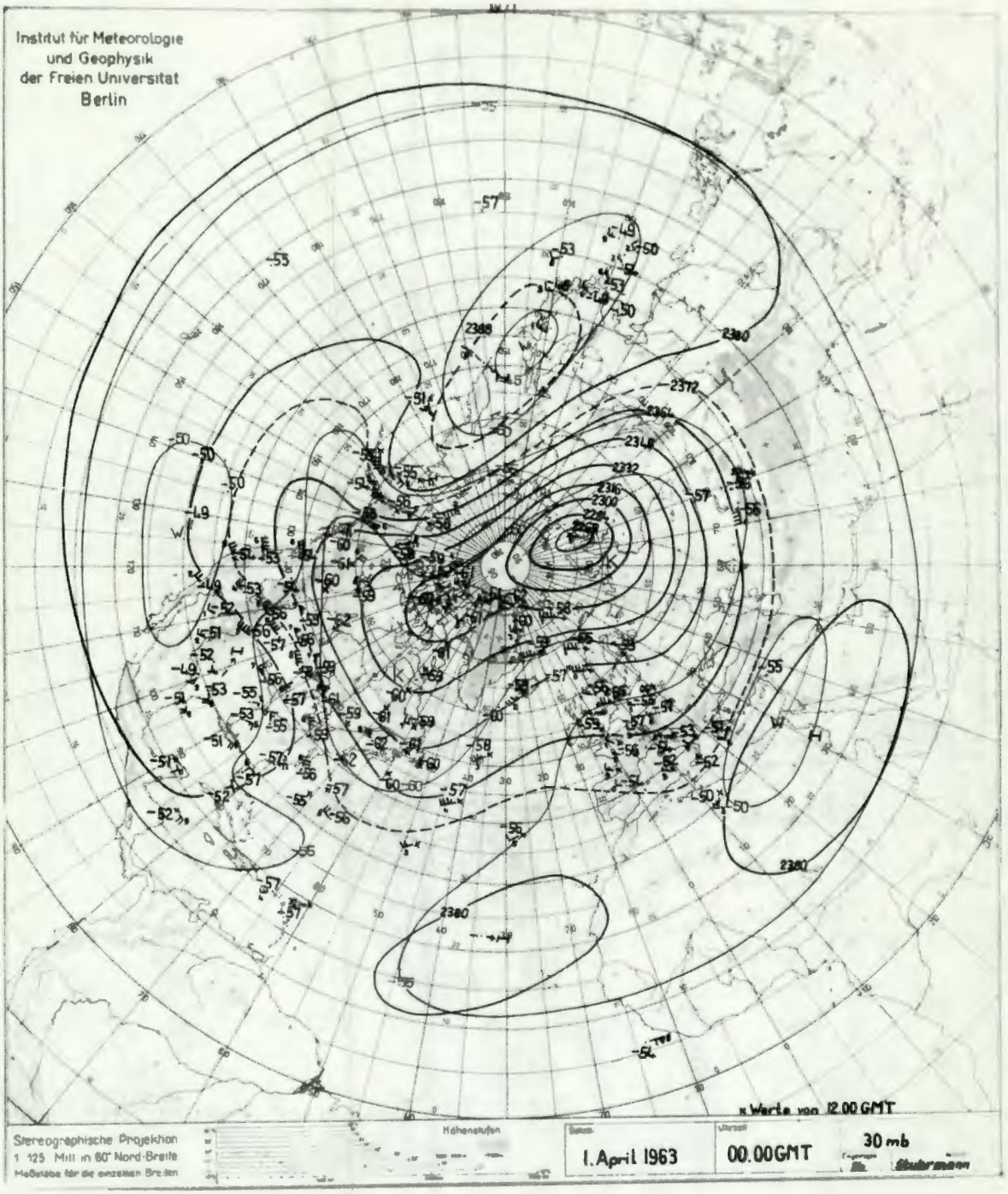

FIG. 20. 30 mb height analysis for 01 April 1963 at 0000GMT (geopotential dekameters).

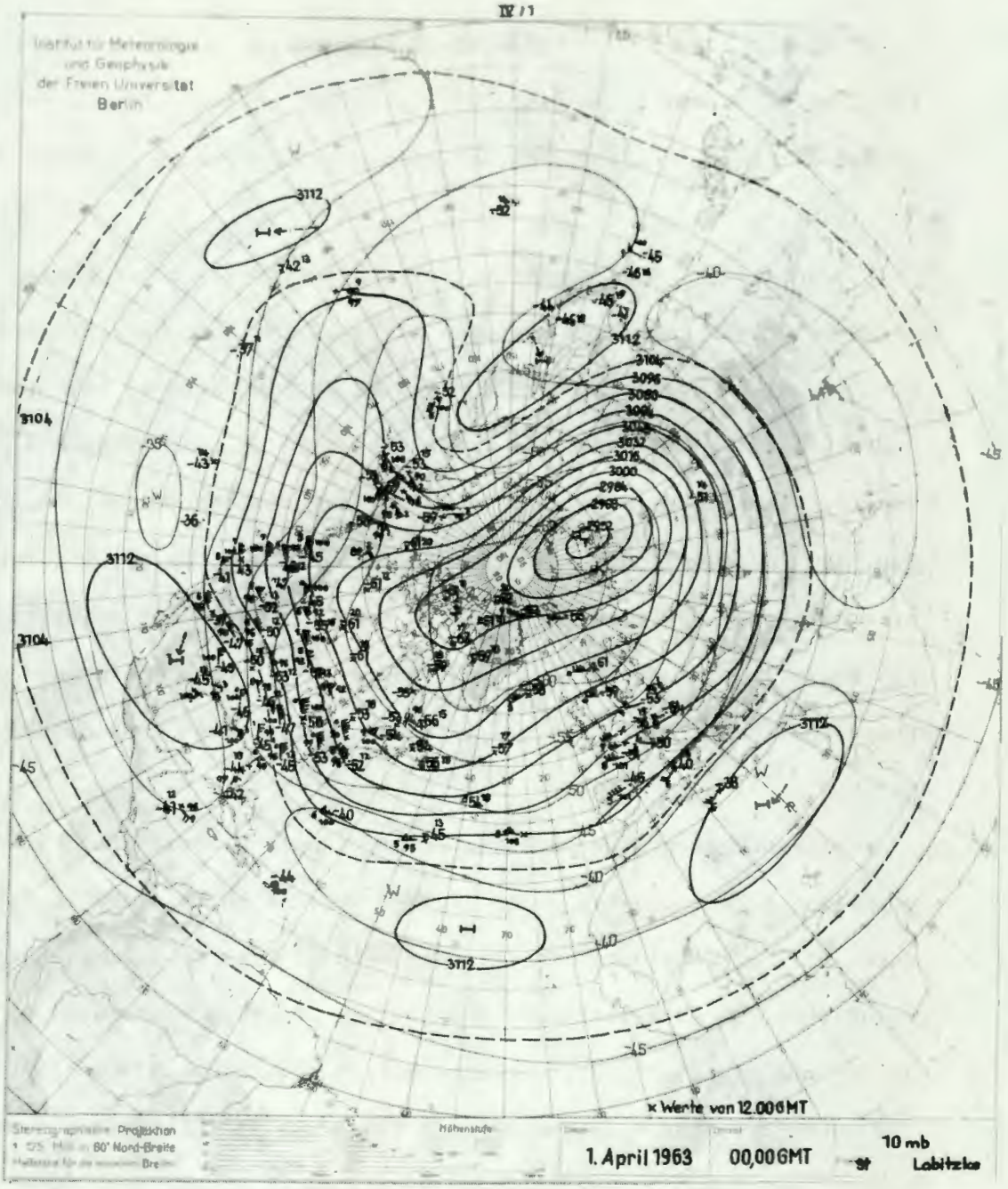

FIG. 21. 10 mb height analysis for 01 April 1963 at 0000GMT (geopotential dekameters).

Figs. 20 and 21 may be considered representative of the period 1-5 April at 30 mb and 10 mb respectively. The cyclonic circulation patterns referred to at 50 mb are even more pronounced at 30 mb and 10 mb.

Therefore, it is apparent that the previously noted areas of negative height anomalies are also areas of cyclonic baroclinic activity, both of which have considerable vertical extent above 50 mb. The predominence of these conditions during the time of this study has important implications regarding the heating function distribution of Fig. 14. Also, it may be noted that this persistence of winter regime stratospheric conditions is during a month in which the transition to the summer regime easterlies is normally in process. It should be noted that the spring reversal is known to have been considerably delayed in 1963.

The development of Section 3 has relagated horizontal transfer processes to a secondary role. Energy generation by diabatic influences will be considered the primary mechanism to be investigated relative to an explanation of the heating function distribution determined by this study. It is apparent from Figs. 13 and 14 that $[\dot{\bar{Q}}]$ and $[\overline{\omega_D}]$ have an opposite sign relationship. Therefore, energy source (sink) regions may generally be located by negative (positive) values of $[\overline{\omega_D}]$. Fig. 13 shows major regions of $[\dot{\bar{Q}}] > 0$ near $45^{\circ}N$ and $85^{\circ}N$, whereas the region of the subpolar vortices is associated with $[\dot{\bar{Q}}] < 0$. The effect of high level ozone irradiation in polar latitudes is considered to play a significant role in the interpretation of the 50 mb diabatic heating distribution resulting from

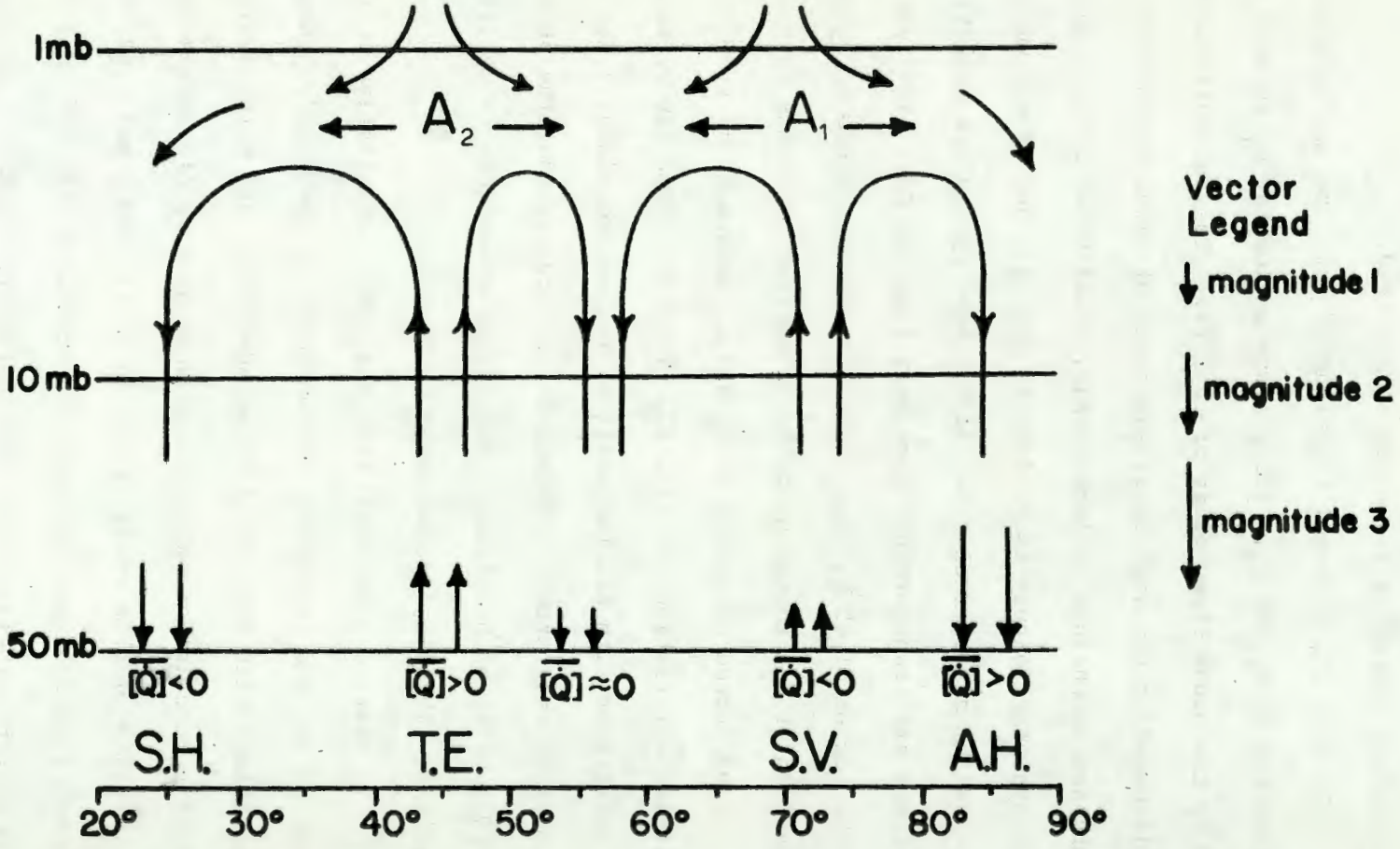

FIG. 22. Schematic model of proposed vertical circulation patterns for 1-5 April 1963. "S.H." is the subtropical high, "T.E." means trough extensions, "S.V." means subpolar vortices, and "A.H." is the Artic high. Vertical motions vectors represent the relative intensity of ω from Fig. 13 ($\omega = \omega_A + \omega_C$).

this study. Fig. 22 schematically presents a proposed vertical circulation model with which the various synoptic and dynamic considerations discussed above may be combined.

In Fig. 22, proposed locations of ozone-radiative heating maxima are at A_1 and A_2. The primary maximum at A_1 is well documented by the ozone climatology of Götz (5). The secondary maximum at A_2 is based on the high level advection of ozone into southwest and southeast extensions of large-scale, broad-based troughs near $45^{\circ}N$. This synoptic feature is evident in Fig. 21, and is presumed to exist at 40-45 km also. Therefore, distinctive cyclonic circulation patterns are transporting ozone away from the Götz high level maximum to the region of $45^{\circ}N$. Radiative warming then produces in situ expansion at A_2, though probably of smaller intensity than at A_1.

The forced outdrafts at A_1 and A_2 maintain the proposed thermal cellular circulations of Fig. 22. These patterns can be shown to be consistent with all the vertical motion and diabatic heating results of this study. Notice, in particular, that the 50 mb warming ($[\overline{Q}] > 0$) at $45^{\circ}N$ indicates the trough extensions to be filling features. This is substantiated by Fig. 23.

It must be understood that Fig. 22 is speculative in the region above 50 mb, and cannot be substantiated by this study. However, the linkage with high level ozone advection, and with existing synoptic circulation patterns, as well as complete agreement with the results of this study, shows an intriguing consistency which may warrant further investigation. Nevertheless, Fig. 22 must be regarded only as a hypothetical circulation pattern which is consistent with the results produced by this study at the level of 50 mb.

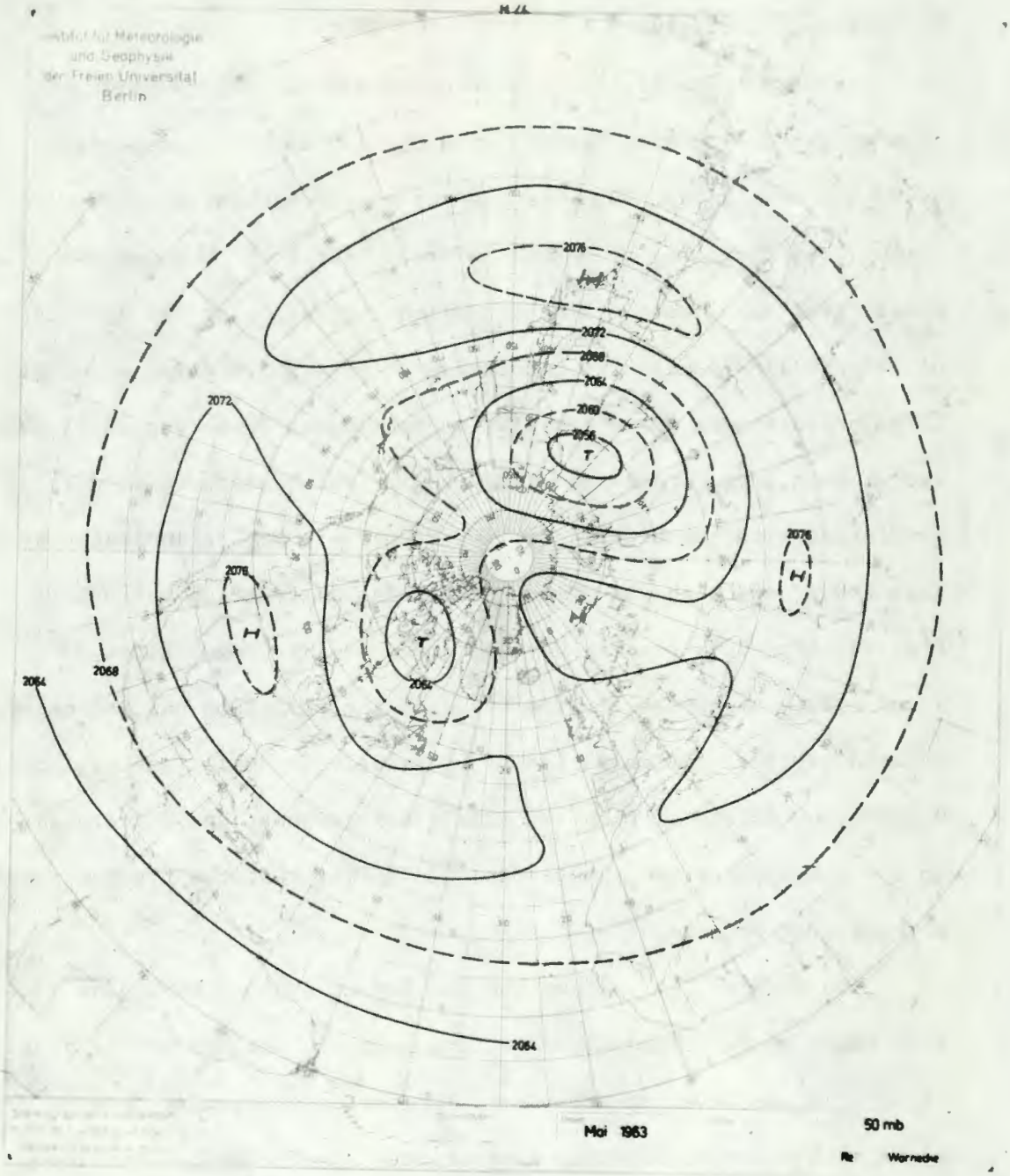

FIG. 23. Mean absolute topography of the 50 mb surface for May 1963 (geopotential dekameters).

9. Concluding remarks

From the results that have been presented, the relationship between vertical motion and diabatic heating is best demonstrated by ω_D. Recall that ω_A was used as a convenience for producing ω_D. Furthermore, it should be noted that both ω_D and ω_A vary widely from ω, but in a manner which suggests that the importance of ω_D is linked with the importance of external heating effects. In polar latitudes where irradiation heating at 50 mb was minor, ω_A was of much larger magnitude than ω_D. This interpretation is consistent with the hemispheric importance of ω_D as indicated by this study, and with the proposed cellular circulation pattern of Fig. 22. Previous studies have produced similar ω_D values as found here, but have evaluated the diabatic effect on adiabatically deduced vertical motion fields to be relatively small [see Paulin (13)]. However, by reason of time and sample differences, and differences in the development of ω_D values, it is felt that the present results are not contradictory.

The Martin χ-field method has led to 50 mb ω-fields and from there to $\dot{Q}$-fields which describe synoptic scale diabatic heating effects in the lower stratosphere. No vertical velocity data is known with which to directly compare the ω-fields produced by Jarrell. However, the ω_A fields of this study afford an order of magnitude check which, it is felt, generally support Jarrell's findings. Furthermore, an averaging technique similar to (39), when applied to the $[\overline{\omega}]$ values of Table 2 yields a hemispheric average of (essentially) zero. But most significantly, these ω-fields

have circulation features which can be reasonably interpreted, and are consistent with synoptic maps for the same time period. Moreover, the $\dot{Q}$ fields resulting from this study show similar consistencies.

These results are considered sufficiently promising to justify further development of the method which produced them, and application of this method at still higher levels; for example, at 10 mb.

BIBLIOGRAPHY

1. Arakawa, A., 1962: Non-geostrophic Effects in the Baroclinic Prognostic Equations. Proceedings of the International Weather Prediction Symposium in Tokyo, Nov. 7-13, 1960, Tokyo, Meteorological Society of Japan, pp. 161-175.

2. Budyko, M. I., 1956: Teplovoi Balans Zemnoi Poverkhnosti (The Heat Balance of the Earth's Surface). Leningrad, Gidrometeorologicheskoe Izdatel'stvo, 255 pp. (Translated by Nina A. Stepanova, U. S. Weather Bureau, Washington, D. C., 1958).

3. Craig, R. A., The Upper Atmosphere, 1965: Academic Press Inc., New York, 509 pp.

4. Davis, P. A., 1963: An Analysis of the Atmospheric Heat Budget. Journal of the Atmospheric Sciences, Vol. 20, No. 1, pp. 5-22.

5. Götz, F. W. P., 1951: Ozone in the Atmosphere, Compendium of Meteorology, Boston, American Meteorological Society, pp. 275-291.

6. Holl, M. M., J. P. Bibbo and J. R. Clark, 1963: Linear Transforms for State-Parameter Structure, Technical Memorandum No. 1, Edition Two, Contract N 228 (62271) 58264, Meteorology International Inc., Monterey.

7. Jarrell, J. D., 1967: Model Computations of Vertical Motion in the Upper Troposphere and Lower Stratosphere from Wind Potential Data. M. S. thesis Department of Environmental Sciences, U. S. Naval Postgraduate School.

8. Martin, F. L., 1964: A Diagnostic Method for Computing the 12-hour Mean Velocity Potential with Special Application to the layer 100-300 mb. Preprint memo. No. 64-6(b), National Center for Atmospheric Research, Boulder.

9. Martin, F. L., 1967: A Formulation of the Lateral Boundary-Condition for the Divergent Component of the Wind Arising From the ω-Equation Applied to the Octagonal Grid. Unpublished paper, Department of Environmental Sciences, U. S. Naval Postgraduate School.

10. McClosky, T. J., 1963: A Diagnostic Study at 100 mb of the Zonally Averaged Fields of Heat Storage, Heat Transport and Diabatic Heating in the Northern Hemisphere During Early April 1963. M. S. thesis, Department of Environmental Sciences, U. S. Naval Postgraduate School.

11. Ohring, G., 1958: The Radiation Budget of the Stratosphere. Journal of Meteorology, Vol. 15, No. 5, pp. 440-451.

12. Pantske, E., 1964: Die Temperatur-und Windverhaltnisse in der Stratosphere uber Berlin im 1. Halbjar 1963. Meteorologische Abhandlungen, Band L, Heft 1, 96 pp.

13. Paulin, G., 1966: Stratospheric Heating Rates. Publication in Meteorology No. 81, Department of Meteorology, McGill University, Montreal.

14. Pressman, J., 1955: Seasonal and Latitudinal Temperature Changes in the Ozonosphere. Journal of Meteorology, Vol. 12, No. 1., pp. 87-89.

15. Staff members, Freien Universität Berlin, 1966: Tägliche Höhenkarten der 50-mb-Fläche sowie monatliche Mittelkarten für das Jahr 1963. Meteorologische Abhandlungen, Band XXXVIII, Heft 2, 102 pp.

16. _____, 1963: Daily and Monthly Northern Hemisphere 30-Millibar Synoptic Weather Maps of the Year 1963. Meteorologische Abhandlungen, Band XXXIX, Heft 2, 100 pp.

17. _____, 1963: Daily and Monthly Northern Hemisphere 10-Millibar Synoptic Weather Maps of the Year 1963. Meteorologische Abhandlungen, Band XL, Heft 2, 98 pp.

18. United States Committee on Extension to the Standard Atmosphere, 1962: U. S. Standard Atmosphere, 1962, U. S. Government Printing Office, Washington, D. C., 278 pp.

INITIAL DISTRIBUTION LIST

		No. Copies
1.	LT W. Rogers, Jr., USN Patrol Squadron Thirty-One Naval Air Station Moffett Field, California 94035	2
2.	Professor F. L. Martin Department of Meteorology & Oceanography Naval Postgraduate School Monterey, California 93940	5
3.	Library Naval Postgraduate School Monterey, California 93940	2
4.	Department of Meteorology & Oceanography Naval Postgraduate School Monterey, California 93940	3
5.	Defense Documentation Center Cameron Station Alexandria, Virginia 22314	20
6.	Naval Weather Service Command Naval Station (Washington Navy Yard Annex) Washington, D. C. 20390	1
7.	Officer in Charge Naval Weather Research Facility Naval Air Station, Building R-48 Norfolk, Virginia 23511	1
8.	Officer in Charge Fleet Numerical Weather Facility Naval Postgraduate School Monterey, California 93940	2
9.	Director, Naval Research Laboratory Attn: Tech. Services Information Officer Washington, D. C. 20390	1
10.	Office of Chief Signal Officer Research and Development Division Department of the Army Washington, D. C. 20310	1
11.	AFCRL - Research Library L. G. Hanscom Field Attn: Nancy Davis/Stop 29 Bedford, Massachusetts 01730	1

12. Program Director for Meteorology — 1
National Science Foundation
Washington, D. C. 20550

13. Office of Naval Research — 1
Department of the Navy
Washington, D. C. 20360

14. Department of Commerce, ESSA — 2
Weather Bureau
Washington, D. C. 20235

15. Bureau of Meteorology — 1
Attn: Library
Box 1289K, G.P.O.
Melbourne, Victoria, Australia 3001

16. International Antartic Meteological Research Center — 1
Box 1289 K, G.P.O.
Melbourne, Victoria, Australia 3001

17. Chairman — 1
Department of Meteorology & Oceanography
New York University
University Heights, Bronx
New York, New York

18. Department of Meteorology & Oceanography — 1
Chairman
University of Hawaii
Honolulu, Hawaii

19. Department of Meteorology — 1
University of California
Los Angeles, California

20. Department of Geophysical Sciences — 1
University of Chicago
Chicago, Illinois

21. Department of Atmospheric Science — 1
Colorado State University
Fort Collins, Colorado

22. Department of Engineering Mechanics — 1
University of Michigan
Ann Arbor, Michigan

23. School of Physics — 1
University of Minnesota
Minneapolis, Minnesota

24. Department of Meteorology — 1
University of Utah
Salt Lake City, Utah

25. National Center for Atmospheric Research — 1
Boulder, Colorado

26. Department of Meteorology & Climatology — 1
University of Washington
Seattle, Washington 98105

27. Department of Meteorology — 1
University of Wisconsin
Madison, Wisconsin

28. Department of Meteorology — 1
Florida State University
Tallahassee, Florida

29. Department of Meteorology — 1
Massachusetts Institute of Technology
Cambridge, Massachusetts 02139

30. Department of Meteorology — 1
Pennsylvania State University
University Park, Pennsylvania

31. Atmospheric Science Branch — 1
Science Research Institute
Oregon State College
Corvallis, Oregon

32. The University of Texas — 1
Electrical Engineering Research Laboratory
Engineering Science
Building 631A
University Station
Austin, Texas 78712

33. Department of Meteorology — 1
Texas A & M University
College Station, Texas 77843

34. Lamont Geological Observatory — 1
Columbia University
Palisades, New York

35. International Antartic Analysis Center — 1
468 Lonsdale Street
Melbourne, Victoria, Australia

36. Department of Meteorology — 1
McGill University
Montreal, Canada

37. Central Analysis Office — 1
Meteorological Branch
Regional Adm Building
International Airport
Dorval, Quebec, Canada

38. Meteorological Office — 1
315 Bloor Street West
Toronto 5, Ontario, Canada

39. Institut fur Theoretische Meteorologie — 1
Freie Universitat Berlin
Berlin-Dahlem
Thiel-allee 49
Federal Republic of Germany

40. Meteorological Service — 1
44, Upper O'Connell Street
Dublin 1, Ireland

41. Department of Meteorology — 1
The Hebrew University
Jerusalem, Isreal

42. Geophysical Institute — 1
Tokyo University
Bunkyo-ku
Tokyo, Japan

43. Department of Meteorology — 1
Instituto de Geofisica
Universidad Nacional de Mexico
Mexico 20, F.F., Mexico

44. New Zealand Meteorological Service — 1
P. O. Box 722
Wellington, G. E., New Zealand

45. Institute of Geophysics — 1
University of Bergen
Bergen, Norway

46. Department of Meteorology — 1
Imperial College of Science
South Kensington
London S. W. 7, United Kingdom

47. Meteorological Office — 1
London R
Bracknell
Berkshire, United Kingdom

48. Commonwealth Scientific and Industrial Research Organization
314 Albert Street
East Melbourne, C. 2, Victoria — 1

49. Division of Engineering and Applied Physics
Room 206, Pierce Hall
Harvard University
Cambridge, Massachusetts — 1

50. Department of Mechanics
The Johns Hopkins University
Baltimore, Maryland — 1

51. Department of Astrophysics & Atmospheric Physics
University of Colorado
Boulder, Colorado — 1

DOCUMENT CONTROL DATA - R&D

(Security classification of title, body of abstract and indexing annotation must be entered when the overall report is classified)

1. ORIGINATING ACTIVITY (Corporate author)	2a. REPORT SECURITY CLASSIFICATION
Naval Postgraduate School Monterey, California	UNCLASSIFIED
	2b. GROUP

3. REPORT TITLE

A Study of the Vertical Motions and of the Diabatic Heating Effects in the Lower Stratosphere During Early April 1963

4. DESCRIPTIVE NOTES (Type of report and inclusive dates)

Thesis

5. AUTHOR(S) (Last name, first name, initial)

ROGERS, Will Jr.

6. REPORT DATE	7a. TOTAL NO. OF PAGES	7b. NO. OF REFS
December 1967	69	18

8a. CONTRACT OR GRANT NO.	9a. ORIGINATOR'S REPORT NUMBER(S)
b. PROJECT NO.	
c.	9b. OTHER REPORT NO(S) (Any other numbers that may be assigned this report)
d.	

10. AVAILABILITY/LIMITATION NOTICES

[redacted]

11. SUPPLEMENTARY NOTES	12. SPONSORING MILITARY ACTIVITY
	School. Naval Postgraduate School Monterey, California

13. ABSTRACT

Based on a vertical motion model derived by Martin (1964), and applied by Jarrell (1967), a method is developed for producing diabatic heating function fields at 50 mb from independently computed fields of diabatic and adiabatic vertical motion. Vertical motions over and above the adiabatically computed part are found to be of major significance in the diabatic heating function calculations. The resulting heating function fields are shown to be compatible with existing synoptic trends at 50 mb and above, for the data period 1-5 April 1963. A proposed circulation linkage involving ozone-heating areas is advanced, which fits all of the mean zonal computations of diabatic heating and of vertical motion into a consistent pattern.

DD FORM 1 JAN 64 1473

14. KEY WORDS	LINK A		LINK B		LINK C	
	ROLE	WT	ROLE	WT	ROLE	WT
geopotential thickness						
Holl stability parameter						
diagnostic vertical motions						
stratospheric omega fields						
diabatic heating function						